Ore Geology Reviews 74 (2016) 151–169

Contents lists available at ScienceDirect

Ore Geology Reviews

journal homepage: www.elsevier.com/locate/oregeorev

Geology of the Jiama porphyry copper–polymetallic system, Lhasa Region, China

Wenbao Zheng [a,b,*], Juxing Tang [a], Kanghui Zhong [c], Lijuan Ying [a], Qiufeng Leng [c], Shuai Ding [c], Bin Lin [a]

[a] Institute of Mineral Resources, Chinese Academy of Geological Sciences (CAGS), Beijing 100037, China
[b] China University of Geosciences, Beijing 100083, China
[c] Chengdu University of Technology, Chengdu 610059, China

ARTICLE INFO

Article history:
Received 3 June 2015
Received in revised form 17 November 2015
Accepted 18 November 2015
Available online 19 November 2015

Keywords:
Geology
Geochronology
Porphyry Cu–polymetallic system
Gangdese Metallogenic Belt
Tibet

ABSTRACT

The Jiama deposit, located in the eastern part of the well-known Gangdese Metallogenic Belt on the Tibetan Plateau, is the largest porphyry Cu–polymetallic system in the region, with the largest exploration budget, and is economically viable in the Gangdese Belt to undergo large-scale development. The deposit is well preserved and has experienced little erosion. The proven resources of the deposit are 7.4 Mt Cu, 0.6 Mt Mo, 1.8 Mt Pb + Zn, 6.65 Moz Au, and 360.32 Moz Ag. The results presented in this paper are based on geological and tectonic mapping, geological logging, and other exploration work performed by members of the Jiama Exploration Project Team over a period of 6 years. We propose that the Jiama porphyry Cu–polymetallic system is composed of skarn Cu–polymetallic, hornfels Cu–Mo, porphyry Mo ± Cu, and distal Au mineralization. The development of skarn Cu–polymetallic orebodies at the Jiama deposit was controlled mainly by the contact zone between porphyries and marbles, an interlayer detachment zone, and the front zone of a gliding nappe structure. The hornfels Cu–Mo and porphyry Mo ± Cu orebodies were controlled mainly by a fracture system related to intrusions, and the distal Au mineralization resulted from late-stage hydrothermal alteration.

On the basis of field geological logging, optical microscopy, and chemical analysis, we verify that the alteration zones in the Jiama deposit include potassic, phyllic, propylitic, and argillic alteration, with a local lithocap, as well as endoskarn and exoskarn zones. The endoskarn occurs mainly as epidote alteration in quartz diorite porphyry and granite porphyry, and is cut by massive andradite veins. The exoskarn includes garnet–pyroxene and wollastonite skarn, in which the mineralogy and mineral chemical compositions display an outward zonation with respect to the source porphyry. From the proximal skarn to the intermediate skarn to the distal skarn, the garnet/pyroxene ratio varies from >20:1 to ~10:1 to ~5:1, the garnet color varies from red-brown to brown-green to green-yellow, and the average composition of garnet varies from $Ad_{80.1}Gr_{18.9}(Sp + Py)_{1.0}$ to $Ad_{76.3}Gr_{23}(Sp + Py)_{0.7}$ to $Ad_{59.5}Gr_{39.5}(Sp + Py)_{1.0}$, respectively. The pyroxene is not as variable in composition as the garnet, and is primarily light green to white diopside with a maximum hedenbergite content of ~20% and an average composition of $Di_{88.6}Hd_{8.9}Jo_{2.5}$. From the proximal skarn to the intermediate skarn to the distal skarn, the mineralization changes from Cu–Mo to Cu ± Mo to Pb–Zn ± Cu ± Au ores, respectively. The wollastonite skarn displays no zonation and hosts mainly bornite mineralization. The Cu and Mo mineralization is closely related to the potassic and phyllic zones in the porphyry–hornfels.

Zircons from four mineralized porphyries yield U–Pb ages of 15.96 ± 0.5 Ma, 15.72 ± 0.14 Ma, 15.59 ± 0.09 Ma, and 15.48 ± 0.08 Ma. The Re–Os ages of molybdenite from the skarn, hornfels, and porphyry are 15.37 ± 0.15 Ma, 14.67 ± 0.37 Ma, and 14.66 ± 0.27 Ma, respectively. The present results are consistent with the findings of previous research on fluid inclusions, isotopes, and other such aspects. On the basis of the combined evidence, we propose a porphyry Cu–polymetallic system model for the Jiama deposit and suggest a regional exploration strategy that can be applied to prospecting for porphyry-skarn mineralization in the Lhasa area.

1. Introduction and exploration history

Porphyry Cu systems usually include porphyry deposits centered on intrusions, skarn, carbonate-replacement, and high- and intermediate-sulfidation epithermal deposits, which supply nearly three-quarters of the world's Cu, perhaps half the Mo and one-fifth of the Au, and minor amounts of Ag, Pb, Zn, and Bi (Sillitoe, 2010). There are extensive

* Corresponding author at: No. 26, Baiwanzhuang Road, CAGS, Beijing 100037, PR China.
E-mail address: zhengwenbao2009@sina.com (W. Zheng).

http://dx.doi.org/10.1016/j.oregeorev.2015.11.024
0169-1368/

porphyry Cu systems in the Gangdese Metallogenic Belt which is the largest porphyry Cu belt in China.

The Jiama porphyry Cu–polymetallic system is located in Metrorkongka County, in the Tibet Autonomous Region of China, approximately 68 km east of Lhasa, the capital city of Tibet (Fig. 1). It is the largest porphyry Cu–polymetallic deposit in Tibet, with the most intensive exploration program, and is also economically viable in the region to be developed on a large scale. Some small-scale lead mining was undertaken in the Jiama area before the 1950s. Geological work conducted from 1951 to 1990, mainly surface trenching in the Jiama ore district, delineated a 3000-m-long belt of Cu–Pb–Zn mineralization. Subsequently, the Tibet Bureau of Mines and Geology conducted a 1:50,000-scale geochemical stream sediment survey and several 1:10,000-scale geophysical surveys (e.g., magnetic susceptibility, and electrical resistivity and polarizability) in the area. The surveys indicated a high potential for considerable Cu, Pb, and Zn ores in the form of skarn-type deposits, and the Lead Mountain area was targeted for exploration. Drilling (to a depth of 10,100 m) was conducted within an area of approximately 2 km^2, and at the end of 2000 a resource of 259 Kt of copper metal and 462.4 Kt of lead metal was estimated (indicated + inferred). Mining activities in the area commenced not long afterward.

In 2007, China National Gold Group Corporation began to acquire and integrate exploration licenses, and commissioned the Institute of Mineral Resources, CAGS, to conduct general geological exploration in the ore district. The Jiama Exploration Project Team first studied the geology, geophysics, and geochemistry of the area, and interpreted the hornfels alteration (over an area of 10 km^2 to the north of Copper Mountain) at the Jiama deposit (Fig. 1) to be closely associated with porphyry emplacement. The ZK1616 drill hole was bored approximately 1 km northeast of the Lead Mountain exploration area (Fig. 1) to search for possible porphyry at depth. The porphyry–hornfels orebody above the ZK1616 drill hole is 490 m thick, with an average copper grade of 0.25% and an average molybdenum grade of 0.05%. The skarn orebody below is 252 m thick and has an average grade of 0.75% Cu, 0.1% Mo, 0.24 g/t Au, and 12.3 g/t Ag. The grade of both Pb and Zn is less than 0.1%. Subsequent exploration work confirmed that the ZK1616 drill hole is near the porphyry–skarn contact zone.

By the end of 2013, drilling in the Jiama ore district had reached a depth of 200,000 m. Four hundred drill holes were completed, and the exploration area was extended to 7 km^2. The exploration results show that the porphyry Cu–polymetallic system is composed mainly of skarn Cu–polymetallic orebodies, and hornfels Cu–Mo and porphyry Mo ± Cu orebodies (Tang et al., 2010, 2013a; Zheng et al., 2010, 2012a). The skarn ore resource accounts for ~60% of the entire deposit, the hornfels ore for ~35%, and the porphyry ore for ~5%. The deposit contains six elements (Cu, Mo, Au, Ag, Pb, and Zn) that can be extracted, and it is highly economical (Table 1).

On the basis of geological–tectonic mapping, geological logging, and other work done by the Jiama Exploration Project Team, the present study describes the geological setting, alteration, and mineralization of the Jiama porphyry Cu–polymetallic deposit, assesses the timing of diagenesis and metallogenesis, establishes a geological model for the system, and proposes a strategy for regional exploration.

2. Regional geological and metallogenic setting

Studies of the tectonics, magmatic rocks, and mineralization of the Gangdese Metallogenic Belt in Southern Tibet have made an

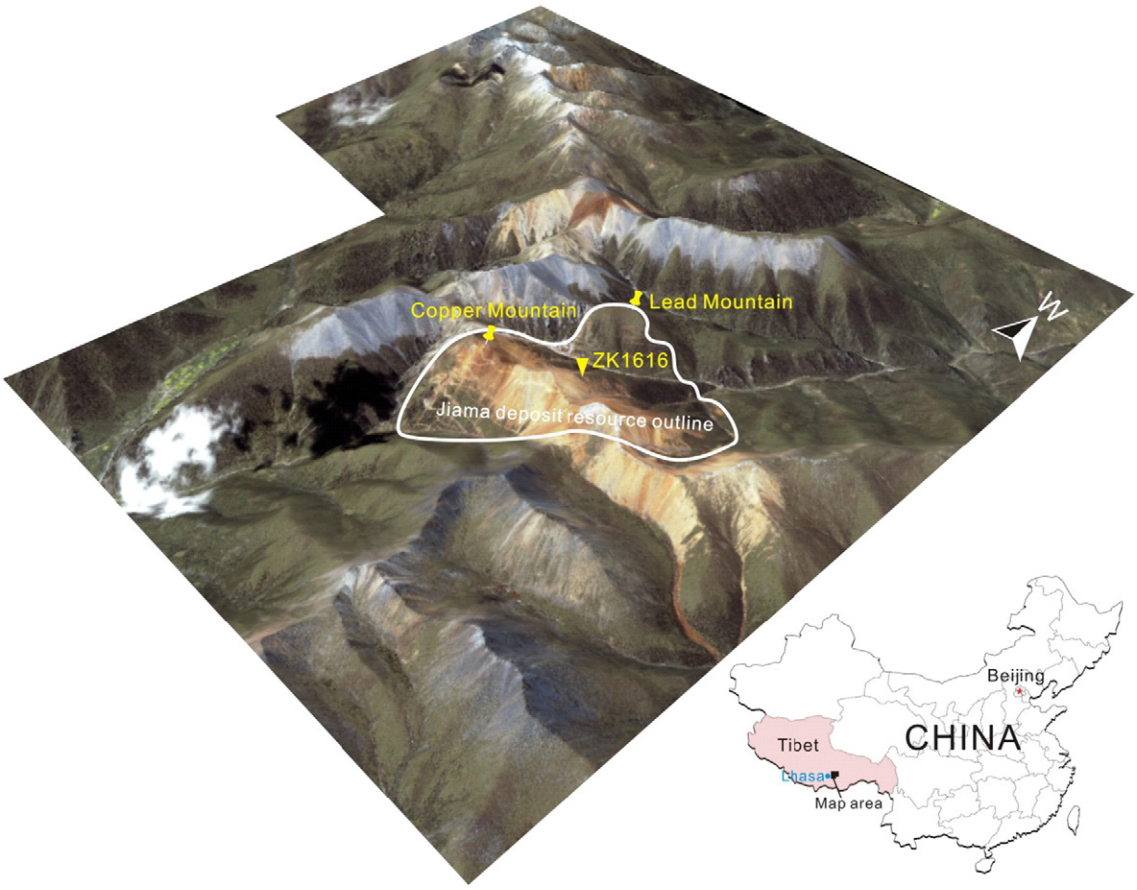

Fig. 1. IKONOS remote-sensing image of the Jiama area. The hornfels alteration zone, which exceeds 10 km^2 in size, is a significant indicator of porphyry systems, and the ZK1616 drill hole has made an important contribution to prospecting in the Jiama deposit.

Table 1
Jiama porphyry Cu-polymetallic system resources (Measured + Indicated + Inferred) (as of November 2013).

Industrial Type		Cu	Mo	Pb	Zn		Au	Ag
Skarn	Quantity (Mt)	621.3						
	Grade (%)	0.64	0.04	0.15	0.09	Grade(g/t)	0.25	14.69
	Metal (Kt)	3972	247	952	543	Metal (Moz)	4.955	293.518
Hornfels	Quantity (Mt)	1184.4						
	Grade (%)	0.27	0.03	0.01	0.01	Grade (g/t)	0.04	1.55
	Metal (Kt)	3155	343	147	118	Metal (Moz)	1.512	58.707
Porphyry	Quantity (Mt)	86.5						
	Grade (%)	0.30	0.04	0.01	0.01	Grade (g/t)	0.07	2.91
	Metal (Kt)	257	35	7	9	Metal (Moz)	0.185	8.09
Totals	Quantity (Mt)	1892.2						
	Grade (%)	0.39	0.03	0.06	0.04	Grade (g/t)	0.11	5.92
	Metal (Kt)	7384	625	1106	670	Metal (Moz)	6.652	360.315

important contribution to our understanding of the greater Tethyan–Himalayan Metallogenic Domain (Chung et al., 2005, 2009; Hou and Cook, 2009, Hou et al., 2013; Mao et al., 2014; Mo et al., 2007; Pan et al., 2012; Wang et al., 2014a, 2014b; Xu et al., 2009; Yin et al., 1994, Yin and Harrison 2000; Zhu et al., 2009, 2011). The belt is bounded by the Meso-Tethyan Bangong–Nujiang suture and the Neo-Tethyan Indus–Yarlung Zangbo suture, and is approximately 2000 km long east–west, and up to 500 km wide north–south (Fig. 2a). Current mineral exploration and research is centered in the south of the Shiquan River–Nam Tso mélange belt, ~600 km from Shigatse city toward Bayi town (Fig. 2b). The mineral deposits in the area are related to the northward subduction of the Neo-Tethyan slab and are of three types: (1) porphyry Cu–Au deposits formed in a subduction setting (180–160 Ma), such as the Xiongcun deposit (Lang, 2012, Lang et al., 2014; Tafti et al., 2009, 2014); (2) porphyry Mo ± W and related skarn Pb–Zn and epithermal Au–Ag deposits formed in a syn-collision setting (70–50 Ma), such as the Sharang and Yaguila deposits (Gao et al., 2011; Tang et al., 2009; Yang et al., 2014); and (3) porphyry Cu–Mo and related skarn Cu–polymetallic deposits formed in a post-collisional setting (20–12 Ma), such as the Qulong and Jiama deposits (Leng et al., 2013; Yang et al., 2009; Ying et al., 2014; Fig. 2b; Table 2). However, the three stages described above do not include the Nuri cluster of mineral deposits, which are located just hundreds of meters from the Indus–Yarlung Zangbo suture. The Nuri cluster includes porphyry- and skarn-type deposits, which host predominantly Cu, Mo, and W ores. Most of the deposits formed between 40 and 23 Ma (Fig. 2b; Table 2), but the Sangbujiala skarn Cu deposit formed at 93.3 ± 4.1 Ma (Zhao et al., 2012). These deposits of the Nuri do not fit with the overall distribution of deposits in the Gangdese Belt, and some scholars have proposed that ore formation in these deposits was related to Neo-Tethyan mid-oceanic ridge subduction (106–86 Ma; Zheng et al., 2014a). There has been little exploration in the Northern Gangdese Belt. The Gaerqiong–Galale Cu–Au cluster of mineral deposits in the northern part of the belt has an ore-formation age of 86.87 ± 0.5 Ma (Tang et al., 2013b; Fig. 2b; Table 2), which may be associated with the southward subduction of the Bangong–Nujiang Ocean crust (Du et al., 2011; Zhu et al., 2011). The recently discovered Jiagang quartz vein-type Mo, W, and Bi deposits in the central Gangdese Belt have an age of 21.37 ± 1.35 Ma (Wang et al., 2006; Fig. 2b; Table 2). These deposits may be localized within an intraplate north–south rift within the Gangdese Belt.

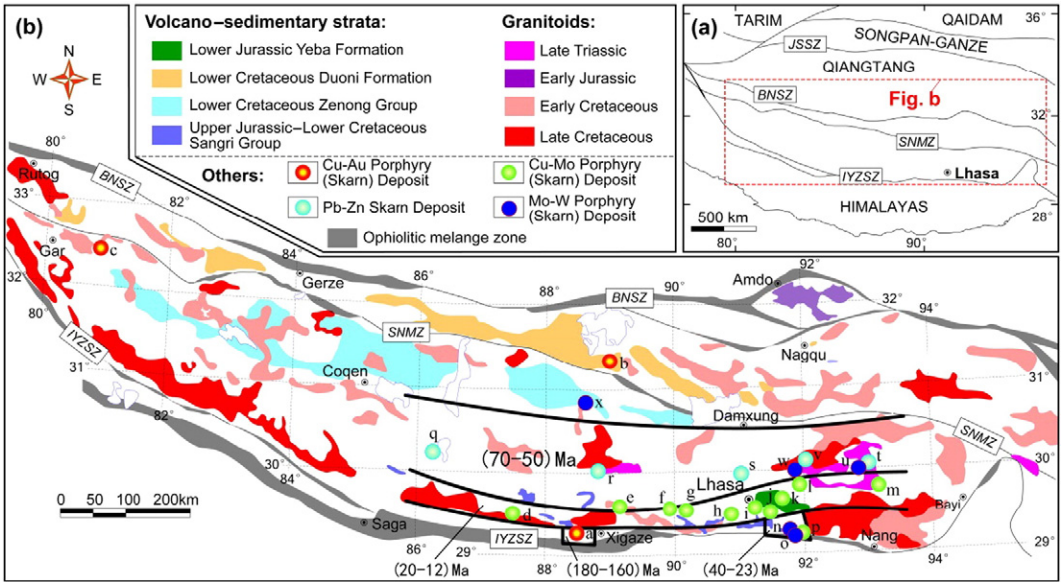

Fig. 2. Location of the Jiama deposit in the Gangdese Metallogenic Belt. (a) The Gangdese Metallogenic Belt in the context of the Tibetan Plateau. (b) Volcano-sedimentary strata, granitoids, and the major porphyry and skarn deposits. Modified from Zhu et al. (2011). Abbreviations: JSSZ = Jinsha suture zone; BNSZ = Bangong–Nujiang suture zone; SNMZ = Shiquan River–Nam Tso mélange zone; IYZSZ = Indus–Yarlung Zangbo suture zone.

Table 2
Molybdenum Re–Os age of main deposits in the Gangdese Metallogenic Belt.

Number	Deposit	Industrial type	Metal	Age(Ma)	Reference
a	Xiongcun	Porphyry	Cu, Au	172.6 ± 2.1, 161.5 ± 2.7	Lang et al., 2014
b	Shesuo	Skarn	Cu (Au, Mo)	116.2 ± 1.9	Zhao et al., 2009
c	Gaerqiong-Galale	Skarn	Cu, Au	86.87 ± 0.5	Tang et al., 2013b
d	Zhunuo	Porphyry	Cu (Mo)	13.72 ± 0.62	Zheng et al., 2007
e	Jiru	Porphyry	Cu, Mo	44.9 ± 2.6, 15.2 ± 0.4	Zheng et al., 2014b
f	Gangjiang	Porphyry	Cu, Mo	12.83 ± 0.11	Leng et al., 2013
g	Tinggong	Porphyry	Cu (Mo)	15.49 ± 0.36	Rui et al., 2004
h	Dabu	Porphyry	Cu, Mo	14.6 ± 0.5	Gao et al., 2012
i	Lakange	Porphyry	Cu, Mo	13.12 ± 0.44	Leng et al., 2015
j	Qulong	Porphyry	Cu (Mo)	16.41 ± 0.48	Meng et al., 2003
k	Jiama	Porphyry-Skarn-Hornfels	Cu, Mo, Pb, Zn (Au)	14.66–15.37	This paper
l	Bangpu	Porphyry-Skarn	Mo, Pb, Zn (Cu)	14.96–16.61	Wang et al., 2012b
m	Tangbula	Porphyry	Mo, Cu	20.9 ± 1.3	Wang et al., 2010
n	Nuri	Skarn	W, Cu, Mo	23.62 ± 0.97	Yan et al., 2010
o	Chengba	Porphyry	Mo (Cu)	30.17 ± 0.94	Sun et al., 2013
p	Sangbujiala	Skarn	Cu	93.3 ± 4.1	Zhao et al., 2012
q	Chagele	Porphyry-Skarn	Pb, Zn (Cu, Mo)	71.5 ± 1.3	Wang et al., 2012a
r	Narusongduo	Skarn-Breccia	Pb, Zn	57.81 ± 0.66 (sericite Ar–Ar)	Ji et al., 2014
s	Xingaguo	Skarn	Pb, Zn (Cu)	56.5 ± 2.5	Tang et al., 2012
t	Yaguila	Porphyry-Skarn	Pb, Zn (Cu, Mo)	65 ± 1.9	Gao et al., 2011
u	Sharang	Porphyry	Mo	52.3 ± 0.3	Tang et al., 2009
v	Mengyaa	Skarn	Pb, Zn (Cu)	60.4–65.8	Wang et al., 2015
w	Hahaigang	Porphyry-Skarn	W, Mo, Pb, Zn (Cu)	63.2 ± 3.2	Li et al., 2014
x	Jiagang	Quartz vein	Mo, W, Bi (Cu)	21.37 ± 1.35	Wang et al., 2006

3. Local geology

3.1. Stratigraphy

Outcrops in the Jiama ore district consist primarily of epicontinental passive clastic–carbonate rocks, including Lower to Middle Jurassic Yeba Formation massive andesites, tuffs, and lens-shaped limestones; Upper Jurassic Duodigou Formation limestones; Lower Cretaceous Linbuzong Formation sandstones and slates; Chumulong Formation quartz sandstones, siltstones, and black shales; and, locally, Quaternary colluvium and alluvium (Fig. 3). The whole-rock compositions of Linbuzong Formation hornfels and Duodigou Formation marbles are presented in Table 3.

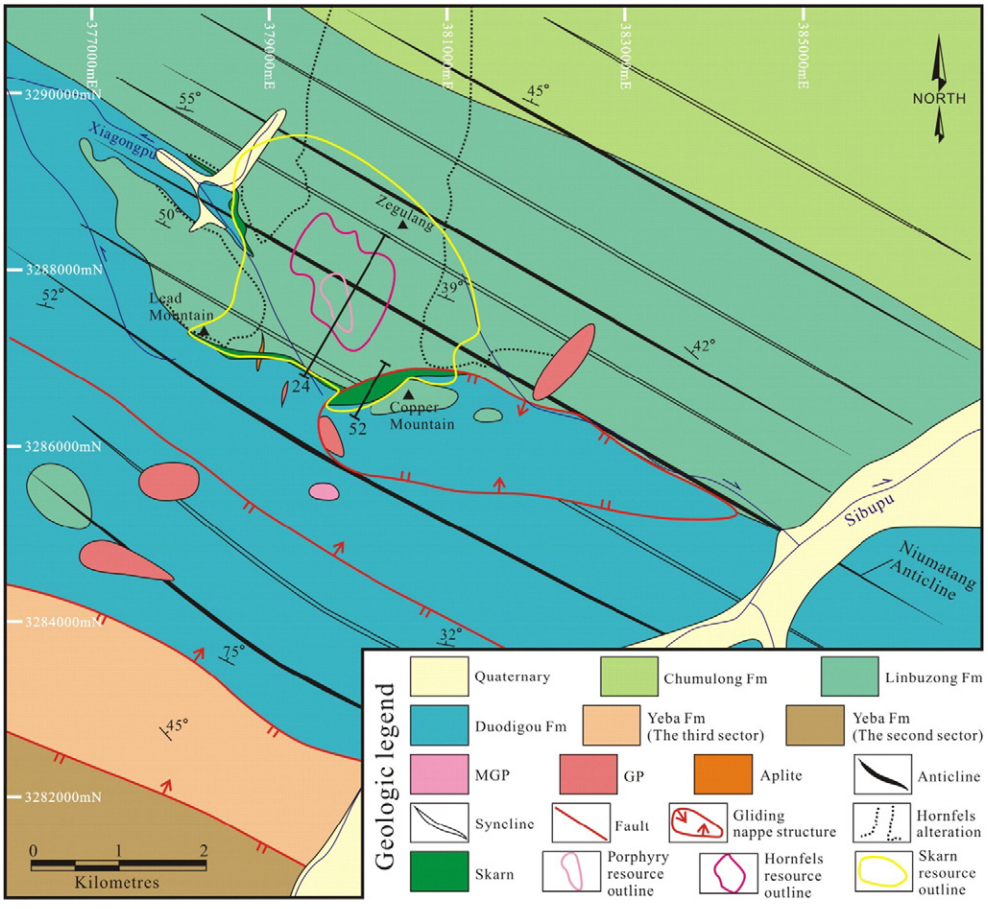

Fig. 3. Geo-tectonic map of the Jiama ore district.

Table 3
Average composition of sedimentary rock units and fresh igneous rocks.

Rock types	Linbuzong Fm. hornfels	Duodigou Fm. marble	QDP	MGP	GDP	GP
Age (Ma)	K_1	J_3	15.96 ± 0.5	15.59 ± 0.1	15.72 ± 0.1	15.48 ± 0.1
No. of analyses	10	13	4	14	8	4
Wt.%						
SiO_2	64.00	6.61	60.40	64.70	67.51	74.63
Al_2O_3	16.54	0.34	15.91	14.77	14.81	12.50
Fe_2O_3	2.63	0.01	2.09	3.16	1.92	1.65
FeO	1.63	na	2.38	1.55	1.56	0.64
CaO	1.32	50.80	4.55	2.89	3.09	0.94
MgO	1.82	0.27	1.82	1.60	1.14	0.29
K_2O	5.16	0.10	2.04	3.52	2.98	4.57
Na_2O	2.45	0.11	4.78	4.82	3.94	2.93
TiO_2	0.75	0.02	0.50	0.41	0.24	0.08
MnO	0.04	0.13	0.06	0.05	0.05	0.03
P_2O_5	0.13	0.03	0.26	0.19	0.14	0.02
Parts per million						
Cu	1676.8	13.0	88.5	265.1	212.1	30.4
Pb	33.3	73.4	30.9	99.6	40.7	40.2
Th	13.6	0.5	5.7	19.5	12.5	19.8
U	2.6	1.5	1.7	5.5	3.8	2.9
Sc	14.0	1.5	9.3	6.4	6.6	5.0
V	116.7	4.5	98.9	63.5	56.6	24.4
Cr	61.2	4.5	19.7	41.8	24.5	21.1
Co	11.2	2.9	12.0	8.8	7.9	3.1
Ni	32.7	14.7	19.1	28.5	17.5	7.1
Zn	39.0	61.6	73.9	122.0	44.5	37.8
Ga	20.0	0.8	19.5	18.2	17.7	14.5
Rb	331.3	7.7	66.8	179.8	136.1	131.2
Sr	90.4	389.0	729.8	511.2	588.5	186.3
Zr	214.7	8.5	115.5	112.3	92.1	82.3
Nb	13.1	0.4	4.0	4.9	5.1	7.8
Ba	298.0	67.9	444.3	734.1	657.5	258.3
Hf	5.4	0.2	2.8	3.1	2.5	2.6
Ta	0.9	0.1	0.3	0.4	0.4	0.8
δEu	0.68	0.82	0.86	0.86	0.88	0.59
A/CNK			0.87	0.87	0.97	1.09
Rb/Sr			0.09	0.35	0.23	0.70

3.2. Igneous rocks

Few intrusions crop out at the surface in the study area. Most of the igneous rocks are evident only in drill core, as dikes or stocks closely related to hornfels in the Copper Mountain–Zegulang area (Fig 3).

3.2.1. Granite porphyry (GP)

Phenocrysts constitute approximately 30%–35% of the GP, and are mainly plagioclase (15%–20%) and K-feldspar (10%), with lesser quartz (1%–5%), biotite (<3%), and amphibole (<2%). The phenocrysts are distributed unevenly through the rock and show intense corrosion. The matrix is felsic, aphanitic, and dominated by K-feldspar (~30%), quartz (>20%), and plagioclase (~10%), with minor biotite (<3%) and amphibole (<2%). The accessory minerals are zircon + titanite + magnetite ± ilmenite ± apatite.

3.2.2. Monzonitic granite porphyry (MGP)

Phenocrysts constitute approximately 30% of the MGP, and are mainly K-feldspar (~15%) and plagioclase (<10%), with minor quartz (~5%) and biotite (<2%). The matrix is felsic, fine-grained, holocrystalline, has a granular texture, and is dominated by K-feldspar (~20%), plagioclase (~20%), and quartz (>20%), with minor biotite (~5%) and amphibole (<2%). The accessory minerals are zircon + titanite + apatite + magnetite ± ilmenite.

3.2.3. Granodiorite porphyry (GDP)

Phenocrysts constitute 20%–25% of the GDP, and are mainly plagioclase (>15%) and amphibole (<5%), with a small amount of quartz (<3%). The matrix is felsic, has a microgranular texture, and is dominated by plagioclase (>45%), quartz (~20%), and amphibole (<15%), with minor biotite (<3%). The accessory minerals are zircon + titanite + apatite + magnetite ± ilmenite.

3.2.4. Quartz diorite porphyry (QDP)

The phenocryst content varies widely in the QDP (<5%–20%). Phenocrysts are mainly plagioclase and amphibole, with minor quartz and biotite. The matrix is dioritic, fine-grained, has a hypidiomorphic-granular texture, and is dominated by plagioclase and amphibole, with lesser quartz, biotite, and K-feldspar. Accessory minerals are zircon + titanite + apatite + ilmenite ± magnetite.

The QDP, GDP, and MGP belong to the calc-alkaline to high-K calc-alkaline series and are quasi-aluminous. These rocks show a systematic enrichment in LILE and depletion in HFSE, weak negative Eu anomalies, and characteristics associated with I-type granites (Table 3; Fig. 4). In contrast, the GP has a high-K, alkaline, peraluminous composition, with negative Eu anomalies and Rb/Sr ratios similar to those of S-type granites (Table 3; Fig. 4).

3.3. Structure

Structure played a vital role in the formation of the Jiama porphyry Cu–polymetallic system. The ore-controlling structures in the Jiama deposit broadly consist of a thrust nappe structure and a gliding nappe structure, as follows.

The thrust nappe structure at Jiama shows progressive south facing deformation characterized by overturned strata comprising Upper Jurassic and Lower Cretaceous clastic–carbonate rocks. The

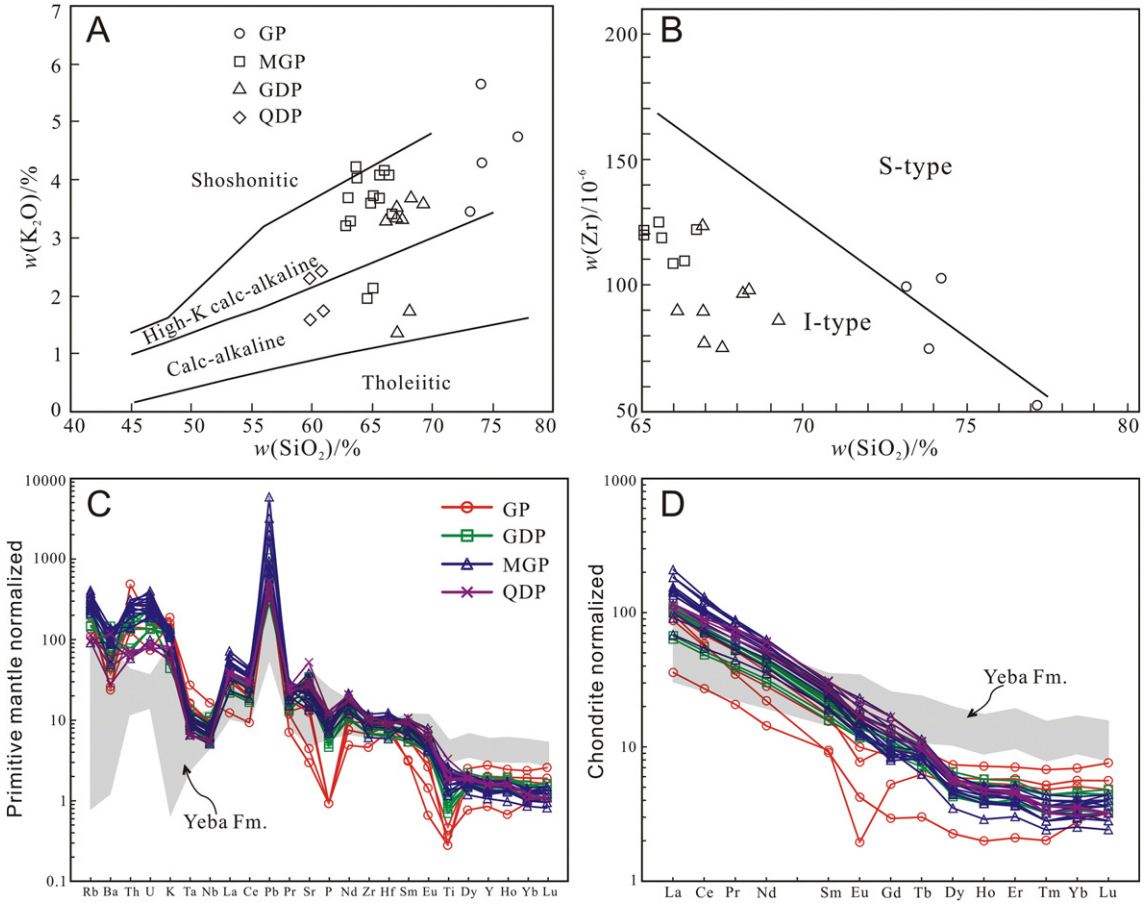

Fig. 4. Data of the Jiama igneous rocks plotted in (A) the K_2O vs. SiO_2 diagram of Le Maitre (2002), and (B) the Zr vs. SiO_2 diagram of Collins et al. (1982). Primitive-mantle-normalized and chondrite-normalized trace element variation diagrams for the Jiama igneous rocks showing (C) similar trace element trends, and (D) listric-shaped REE patterns, indicating fractionation of the magma during ascent through the crust (normalizing values are from Sun and McDonough, 1989). Yeba Formation data are from Zhu et al. (2008) and other data are from Table 3.

~50 Ma age of deformation (Zhong et al., 2012) is close to the time of India–Asia continental collision (Mo et al., 2002, 2007; Yin and Harrison, 2000). The Yeba Formation in the footwall of the nappe is dominated by a series of overturned folds with north-dipping axial surfaces. The nappe structure can be divided from south to north into a quasi in situ system with a front zone, an intermediate zone, and a rear zone (Duan et al., 2014). The Jiama deposit lies in the front and intermediate zones of the nappe structure. The nappe structure led to the development of an interlayer detachment zone between the Linbuzong Formation and the Duodigou Formation, and the intense rock deformation at the bottom of the Linbuzong Formation provides important evidence for the existence of an interlayer detachment fault (Duan et al., 2014; Zhong et al., 2012). The Niumatang overturned anticline in the nappe structure was the primary control on porphyry intrusion and on the formation of the 1# skarn, hornfels, and porphyry orebodies (Fig. 3).

The gliding nappe structure is only developed in the Copper Mountain region of the ore district, in an area covering 4 km^2 (Fig. 3). This structure developed as a result of northward slippage of the unstable high anticline block that was formed by thrust deformation (Zhong et al., 2012). The gliding nappe is only discernible at the peak of Copper Mountain, where only Duodigou Formation limestone and Linbuzong Formation slate (<100 m thick) are present. The gliding nappe can be divided into three zones from north to south: the front zone, the intermediate zone, and the rear zone (Zhong et al., 2012). The front zone has many Z-folds and cleavage structures, which provided sufficient space for the transport and deposition of ore-forming fluids, and controlled the formation of the 2# skarn orebody.

4. Deposit geology

4.1. Orebody types and geometries

The Jiama deposits mainly comprise Cu–polymetallic skarn, Cu–Mo hornfels, and Mo ± Cu porphyry mineralization (Fig 5). The different structural settings described above further define two subtypes of skarn mineralization, referred to as 1# skarn and 2# skarn.

The 1# skarn orebody formed at the contact between porphyry and marble, as well as in the interlayer detachment zone between the Linbuzong Formation hornfels and the Duodigou Formation marbles (Fig. 6A). The orebody occurs as a lamellar, or thick plate and generally lies at an elevations of 4000–5000 m. It strikes west-northwest and dips to the northeast. The upper part of the orebody dips at a steep angle (on average 60°–80°), whereas the lower part is much flatter, with an average dip of 10°–30° (Fig. 6A). The 1# skarn orebody is approximately 3000 m long in the strike direction and 2500 m wide in the dip direction (Fig. 3). The thickness of the skarn orebody that is controlled by the interlayer detachment zone is generally 10 to 50 m, but reaches 50 to 100 m in the anticlinal core. The thickness of the skarn orebody that is controlled by the intrusive body and marble contact belt is typically greater than 100 m, with a maximum of 328 m.

The 2# skarn orebody is lens-shaped and is located in the front zone of the Copper Mountain gliding nappe, at elevations of 4600–5100 m. The orebody strikes east–west, dips south at 50°–80° (Fig. 7), and is generally over 100 m thick. The Cu resource is estimated at 0.5 Mt at a grade of 0.98% Cu, which is suitable for open-pit mining. In the middle to rear

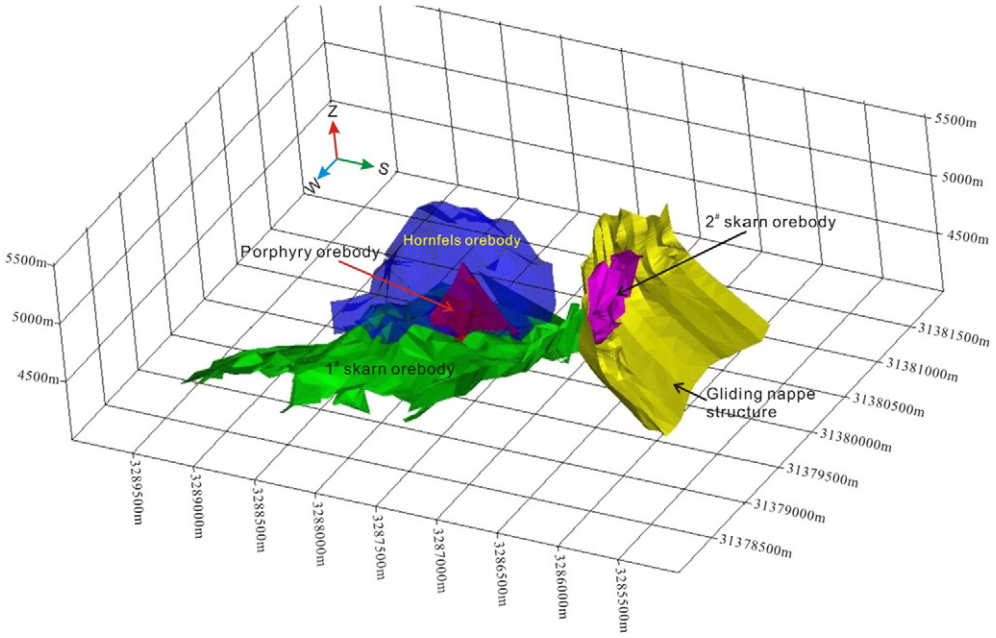

Fig. 5. 3-D view of orebodies in the Jiama porphyry copper–polymetallic system, including the 1# skarn orebody, the 2# skarn orebody, the porphyry orebody, and the hornfels orebody.

of the gliding nappe, a small (<10 m) lens-shaped skarn intersected by a single drill hole is interpreted to display a secondary fold morphology.

The hornfels orebody, which is located at 4300–5200 m elevation between Zegulang and Lead Mountain, strikes NW–SE with a subvertical dip over a distance of 1200 m. In drill hole ZK3217, the body is up to 940 m thick and has an average grade of 0.26% Cu and 0.051% Mo.

The porphyry orebody, located between Zegulang and Lead Mountain at an elevation of <4800 m, is interpreted (from 10 drill holes) as a swarm of QDP, GDP, MGP, and GP dikes that describe an cone shape. The body is elongate north–south, 900 m long, and extends >600 m vertically.

4.2. Ore characteristics

Most of the Jiama deposit consists of sulfide ore, and the zone of oxidation extends upward to just 20 m below the surface.

The hypogene ore minerals are dominated by chalcopyrite and molybdenite, which account for 1%–2% of the primary ore in the hornfels and porphyry orebodies. Tetrahedrite, galena, sphalerite, and native gold are also included in the 1%–10% primary ore of the skarn. Bornite occurs in the wollastonite skarn. Hypogene copper and molybdenum minerals occur in various styles: (1) disseminated in the host rocks as <1 mm anhedral to subhedral crystals that replace feldspar and other minerals, or as clot-like aggregates with hydrothermal biotite and oxide minerals; (2) in veins of <1 mm to several centimeters wide, with quartz, pyrite, and other hypogene minerals; and (3) in skarn. Sphalerite, galena, and chalcopyrite are commonly disseminated, whereas bornite and chalcopyrite also occur as massive ores.

Gangue constitutes 98%–99% of the porphyry and hornfels ore, and 90% of the skarn ore. This consists of primary rock-forming and hydrothermal minerals, including plagioclase, quartz, micas, chlorite, epidote, amphibole, garnet, pyroxene, calcite, anhydrite, aluminum-silicate-sulfate, and accessory minerals.

4.3. Hydrothermal alteration

The major alteration types present in the Jiama porphyry Cu–polymetallic system are potassic, phyllic, argillic, propylitic, and skarn alteration.

4.3.1. Potassic alteration

Potassic alteration occurs mainly in ore-bearing porphyry dikes or in hornfels in contact with porphyries. The alteration zone wide extending into the hornfels is generally less than 500 m, whereas potassic-altered rocks occur in the skarn in contact with the dike, albeit with a small range (generally less than 100 m from the dike). Hydrothermal biotite is the dominant potassic mineral in the zone. There are two main styles of potassic alteration: (1) quartz + biotite + chalcopyrite ± plagioclase ± albite ± pyrrhotite ± pyrite ± magnetite ± molybdenite veins, developed in porphyry, hornfels, and skarn (Fig. 8A); and (2) fine-grained hydrothermal biotite, typically occurring as aggregates with chalcopyrite (<0.5 mm), replacing amphibole and plagioclase as pseudomorphs (Fig. 8B). Most of the quartz veins in the potassic zone are B-type veins; A-type veins are rare.

4.3.2. Phyllic alteration

Phyllic alteration occurs mainly in the hornfels above the potassic alteration zone, and in some porphyry dikes, as sericite and substantial quartz. There are two styles of phyllic alteration: (1) quartz + sericite + pyrite ± chalcopyrite ± calcite ± anhydrite veins in the hornfels; and (2) partial metasomatism of the plagioclase phenocrysts in the porphyry (Fig. 8C). D-type veins dominate in the phyllic alteration zone, with lesser B-type veins. Sulfide minerals in the D-type veins show a strong spatial zonation, from central chalcopyrite-rich veins cutting potassic alteration, grading vertically (Fig. 8D) to pyrite–chalcopyrite veins, and finally to pyrite-dominated veins (Fig. 8E) containing variable amounts of galena, sphalerite, tetrahedrite, and rhodochrosite (Fig. 8F).

4.3.3. Argillic alteration

Argillic alteration occurs in the upper section of the hornfels and in some porphyry dikes, and overlies the phyllic zone. Kaolin and illite alteration, caused by intense deformation, are dominant in the hornfels. Feldspar phenocrysts, which ultimately form kaolin, are commonly destructively altered in porphyry dikes. At the top of the argillic zone, approximately 50 m from the surface, a lithocap of approximately 0.01 km^2 in area has formed. This zone locally contains alunite (Fig. 8G) and is characterized by porous secondary quartz (Fig. 8H).

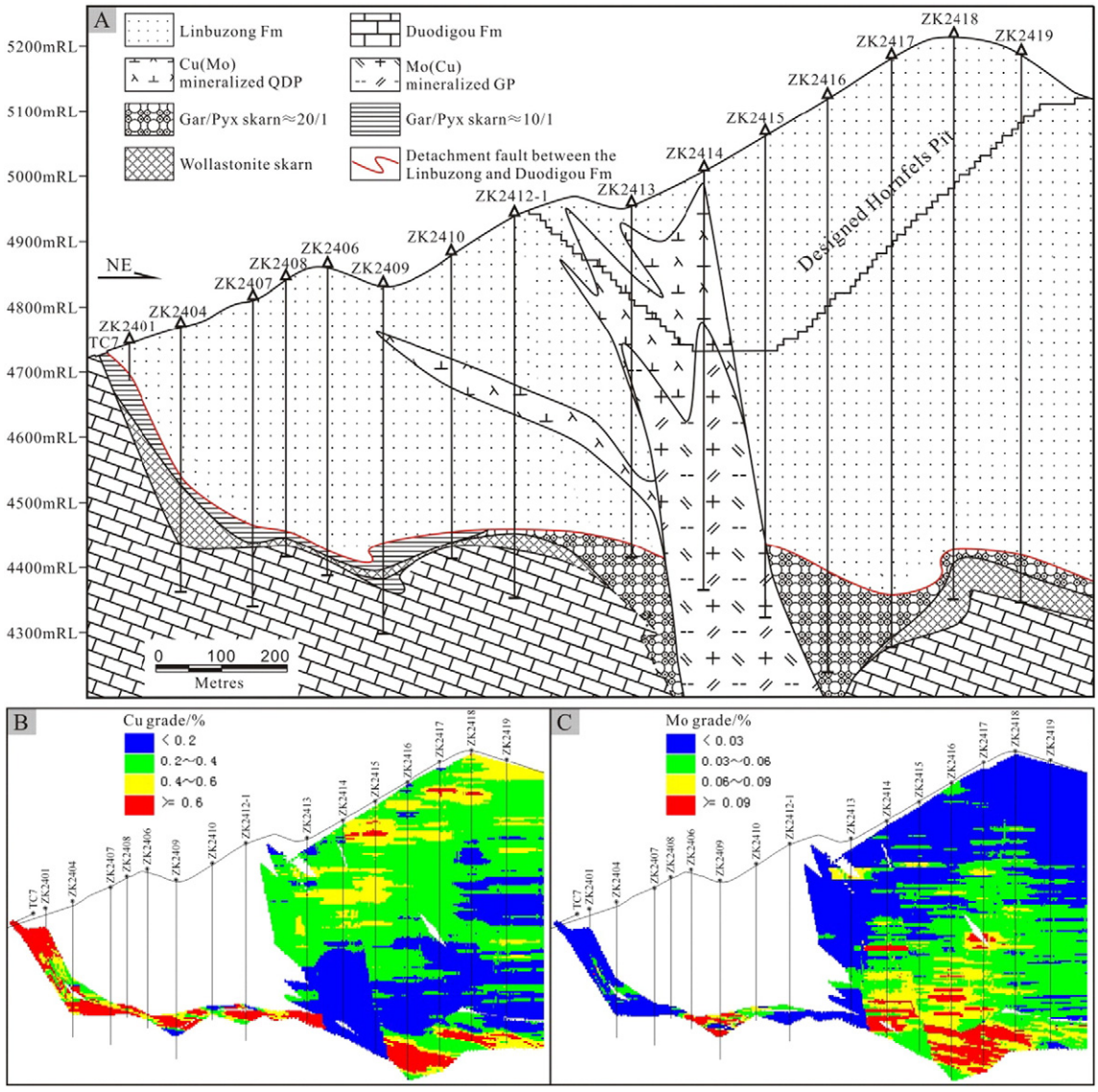

Fig. 6. No. 24 cross-section through the center of the porphyry and hornfels orebodies. (A) Geologic cross-section. (B) and (C) Block diagrams showing the grade in the section shown in (A). The distribution of the Mo and Cu grades in the hornfels–porphyry orebody shows an obvious "upper Cu and lower Mo" feature. The location of the section line is shown in Fig. 3.

4.3.4. Propylitic alteration

Propylitic alteration occurs on the periphery of the potassic and phyllic zones, and is characterized by abundant hydrous minerals. There are three styles of propylitic alteration: (1) quartz + epidote + chlorite + pyrite ± actinolite ± chalcopyrite veins, which commonly occur in the hornfels and porphyry (Fig. 8I); (2) quartz + chlorite + biotite + chalcopyrite + pyrite that are disseminated in the hornfels (under such conditions, the chalcopyrite is relatively abundant; Fig. 8J); and (3) chlorite and epidote derived from partial metasomatism of plagioclase phenocrysts in the porphyry.

4.3.5. Skarn

Skarn is the most important ore-bearing rock in the Jiama deposit and includes endoskarn and exoskarn. The endoskarn occurs mainly in contact with GP or QDP. The skarn in contact with GP is cut by anhydrite veins (Fig. 8K), whereas the QDP contact skarn is dominated by epidote alteration (Fig. 8L). The exoskarn can be subdivided into prograde skarn and retrograde skarn. The former is dominated by garnet, pyroxene, and wollastonite, whereas the latter is characterized by amphibole + epidote + calcite + anhydrite + sulfide (Fig. 8M). Three zones can be identified in the prograde skarn from the porphyry contact zone outwards: proximal skarn, intermediate skarn, and distal skarn (Figs. 6, 7). Wollastonite occurs in the contact zone of the marble, which generally lies below the three aforementioned zones and differs from the three other zones in terms of mineral associations and mineral compositions (Figs. 6, 7). Garnet/pyroxene ratios and the color and compositional zonation of the garnet are variable, both at a scale of individual crystals and throughout the prograde skarn. From the proximal skarn through the intermediate skarn to the distal skarn, garnet/pyroxene ratio ranges from >20:1 to ~10:1 to ~5:1; garnet color ranges from red-brown to brown-green to green-yellow; and the average composition of garnet ranges from $Ad_{80.1}Gr_{18.9}(Sp + Py)_{1.0}$ to $Ad_{76.3}Gr_{23}(Sp + Py)_{0.7}$ to $Ad_{59.5}Gr_{39.5}(Sp + Py)_{1.0}$, respectively (Fig. 9). Pyroxene is not as variable in character as garnet. It consists mainly of light green to white diopside with a maximum hedenbergite content of ~20% and an average composition of $Di_{88.6}Hd_{8.9}Jo_{2.5}$ (from 36 electron microprobe analyses; Fig. 9). At the margin of the skarn, the composition of pyroxene in some sections is ~60% hedenbergite. An idealized skarn alteration zonation pattern for the Jiama deposit is presented in Fig. 10.

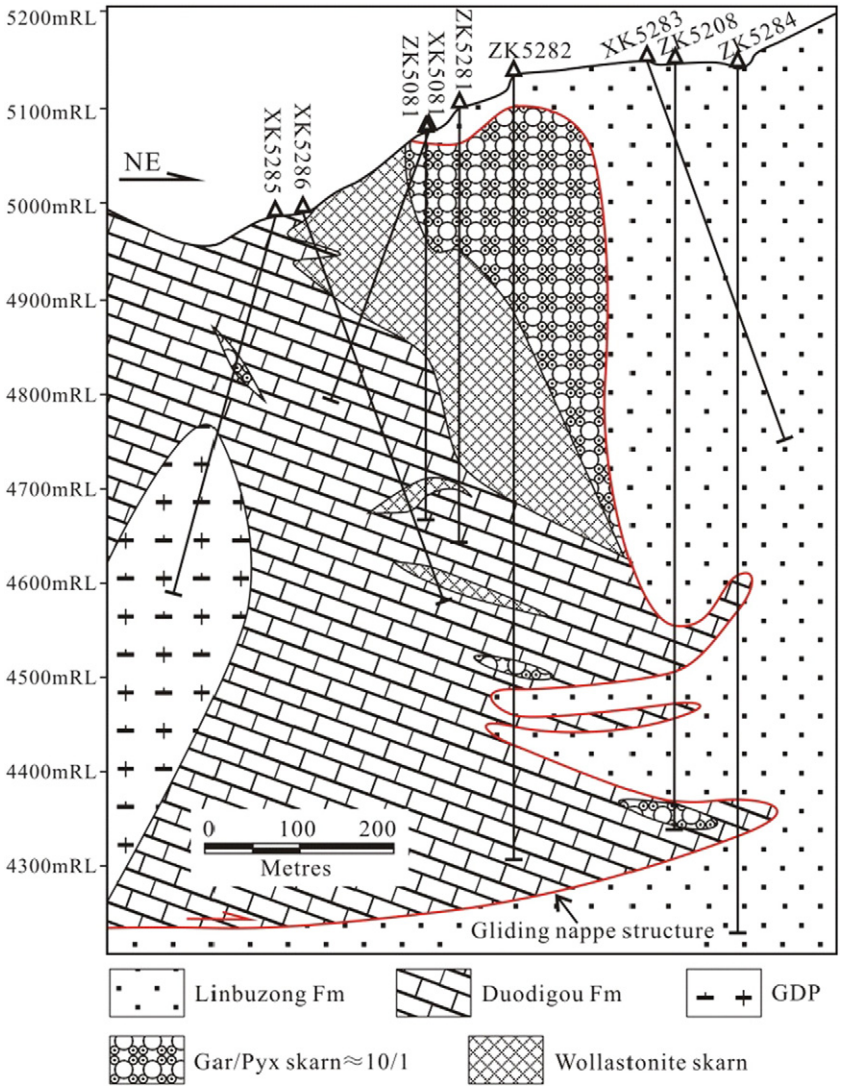

Fig. 7. No. 52 cross-section through the gliding nappe structure, showing the front of the gliding nappe structure that controls the occurrence of the 2# skarn orebody. The location of the section line is shown in Fig. 3.

4.4. Mineralization

4.4.1. Cu mineralization

In the porphyry and hornfels portions of the Jiama deposit, above an elevation of 4700 m (Fig. 6B), Cu mineralization is dominated by disseminated and veinlet chalcopyrite, whereas in the skarn it occurs as massive, disseminated and vein chalcopyrite with bornite and a small amount of vein tetrahedrite. Cu mineralization in the skarn occurs distributed throughout the middle–upper zone of the 1# skarn orebody, and is dominant in the 2# skarn orebody. There are three main stages of copper mineralization in the Jiama deposit: (1) the major metallogenic stage, which produced disseminated-veinlet chalcopyrite mineralization in the upper section of the porphyry and hornfels (Fig. 11A, B), and disseminated, vein, and massive copper mineralization in the skarn (Fig. 11C, D); (2) an intermediate stage, which formed stockwork copper and molybdenum mineralization in the hornfels and porphyry (Fig. 11E); and (3) late-stage near-vertical vein chalcopyrite in the hornfels, porphyry, and skarn (Fig. 11F).

4.4.2. Mo mineralization

The porphyry and hornfels host veined molybdenite, and the skarn hosts disseminated molybdenite, both below an elevation of 4700 m (Fig. 6C). There are two stages of Mo mineralization: (1) disseminated and stockwork in the hornfels, porphyry, and skarn, which occurred later than the first stage of Cu mineralization (Fig. 11G); and (2) vein Cu and Mo mineralization, which occurred at the same time as the second stage of Cu mineralization.

4.4.3. Pb–Zn mineralization

Pb–Zn mineralization occurs mainly in the skarn, and is dominated by banded and disseminated galena + sphalerite. It is found above an elevation of 4800 m, and is distributed throughout the outer zone of the entire 1# skarn orebody, although a small amount of Pb–Zn mineralization occurs in the upper part of the 2# skarn orebody. Galena, sphalerite, and chalcopyrite show a paragenetic sequence discernible in solid solution textures between sphalerite and chalcopyrite (Fig. 11H, I). Therefore, the timing of Pb–Zn mineralization is similar to that of the main stage of Cu mineralization.

4.4.4. Au mineralization

Au and Ag are hosted mainly within chalcopyrite, bornite, and other Cu minerals, and are by-products of Cu extraction. Preliminary data suggest that the Au in the skarn margin is of economic significance (Table 4). The distal Au mineralization has three styles: (1) The gold orebody in the distal zone of the 1# skarn, encountered in drill holes ZK4702 and ZK4703 in the northwest region of the ore district. Here

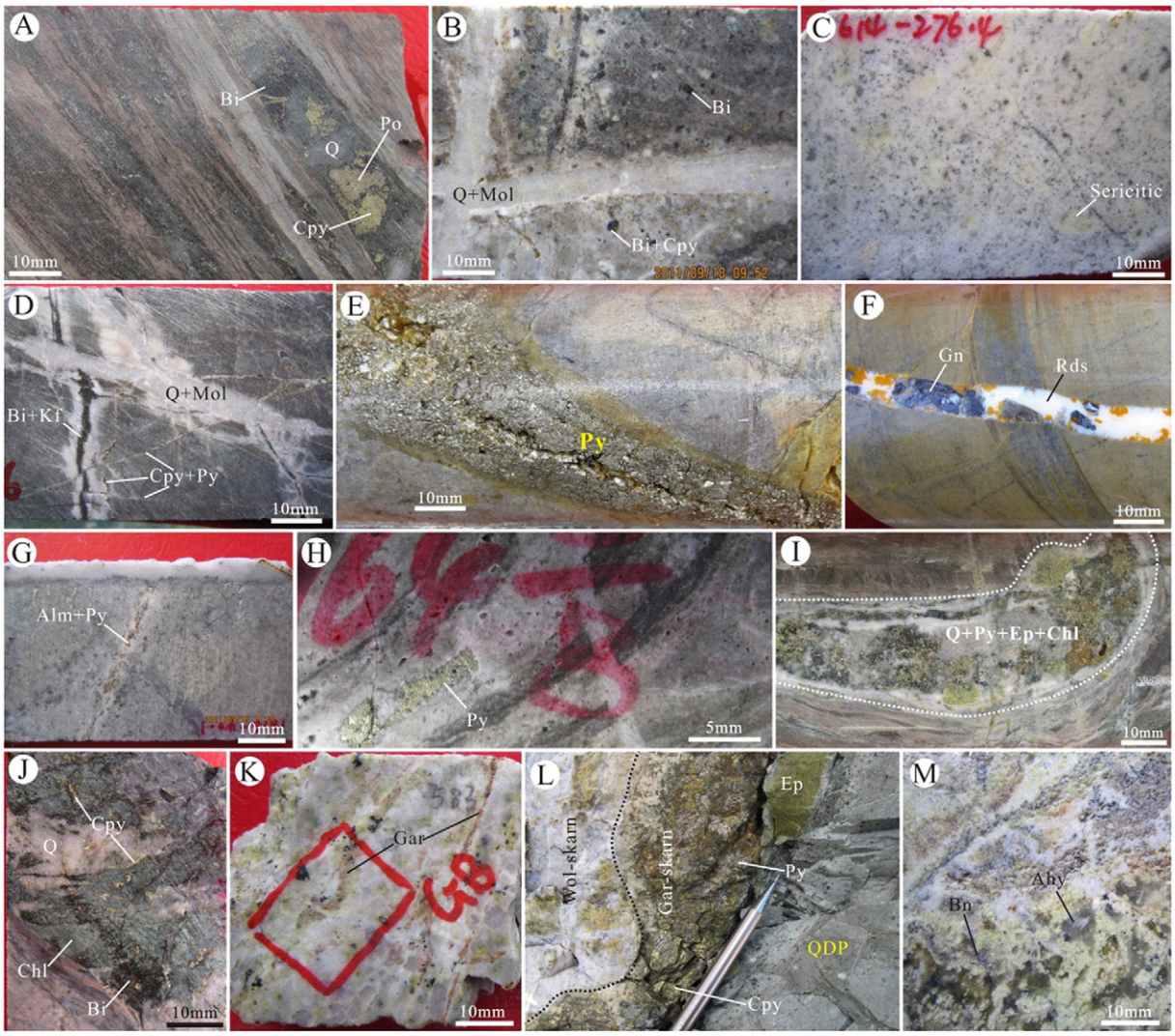

Fig. 8. Alteration features of the Jiama Cu–polymetallic system. (A) Q + Bi + Cpy + Po veins in the potassic zone of the hornfels. (B) Fine-grained hydrothermal Bi and Cpy aggregates replacing Am and Pl phenocrysts in the QDP, while retaining phenocryst shapes. (C) Disseminated Ser is widespread in the GDP, with intensive replacement of Pl phenocrysts occurring locally. (D) The base of the phyllic zone, where early Bi + Kf veins are cut by Cpy + Py veins. (E) The middle and upper parts of the phyllic zone, showing widespread D veins dominated by Py. (F) Low-temperature Rds + Gn veins in the upper part of the phyllic zone. (G) Alu + Py veins in the argillic zone. (H) Porous quartzite in the lithocap of the upper hornfels. (I) Typical Q + Ep + Chl + Py veins in the propylitic zone. (J) Massive Chl and hydrothermal Bi in the propylitic zone, which is enriched in Cpy. (K) The GP is altered in the endoskarn and cut by Ad skarn veins. (L) The contact zone between QDP and skarn — the QDP is affected by epidotization and altered to form the endoskarn. (M) Retrograde alteration skarn occurs in the form of Q + Ahy + sulfides. Q = quartz, Bi = biotite, Cpy = chalcopyrite, Po = pyrrhotite, Am = amphibole, Pl = plagioclase, Ser = sericite, Kf = K-feldspar, Py = pyrite, Rds = Rhodochrosite, Gn = galena, Alu = alunite, Ep = epidote, Chl = chlorite, Ad = andradite, Ahy = anhydrite, and Bn = bornite.

the skarn is dominated by hedenbergite, has intense silicic alteration, and the sulfide association is pyrite + native gold; (2) The gold orebody in the QDP, recognized in drill hole ZK4504 in the northwest region of the ore district. This occurs as veins in the QDP, and the mineral association is quartz + calcite + pyrite + sericite + native gold (Fig. 11J); and (3) The gold orebody in the distal skarn intersected in drill holes ZK8801 and ZK8806 in the southeast region of the ore district. Gold mineralization shows intense actinolite, chlorite, and silica alteration, and sulfides are mainly massive pyrrhotite + chalcopyrite + pyrite + native gold (Fig. 11K, L). This mineralization type is not spatially connected with the 1# skarn orebody or 2# skarn orebody. Distal Au mineralization developed later than Cu–Mo mineralization throughout the deposit, and is the product of late-stage hydrothermal alteration (Zheng et al., 2012b; Zhong et al., 2011).

In terms of metal zoning, an obvious "upper copper, lower molybdenum" is present in the hornfels and porphyry orebodies (Fig. 6B, C). The skarn orebody shows the following zoning outwards from the porphyry contact: Cu–Mo, Cu ± Mo, Pb–Zn, and finally Au mineralization (Fig. 12).

5. Sampling and analytical methods

5.1. Zircon

5.1.1. Sample selection

Four types of igneous rocks associated with the mineralization were sampled in the ore district to use for zircon U–Pb dating. The samples are TSCC-14 (QDP), ZK813-1 (GDP), ZK813-2 (MGP), and ZK2414 (GP). Apart from the sample of QDP, which was collected from the Copper Mountain open pit, the samples were taken from drill core.

5.1.2. Methodology

Individual zircon crystals were hand-picked, mounted in epoxy resin, and polished to remove the upper third of the grain. Prior to isotope analysis, all grains were photographed under both transmitted and reflected light, and subsequently examined under cathodoluminescence (CL). Isotopic ratios were analyzed by laser ablation-inductively coupled plasma-mass spectrometry (LA-ICP-MS) at the MRL Key Laboratory of Metallogeny and Mineral Assessment,

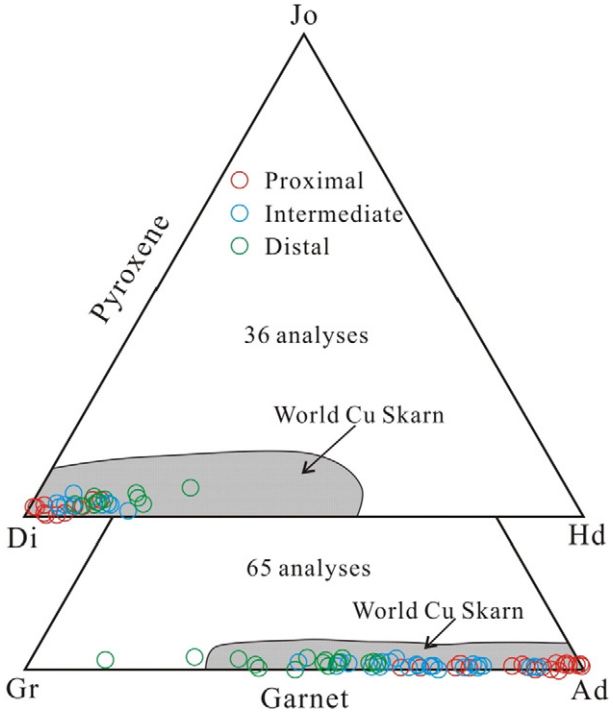

Fig. 9. Ternary plot of Jiama skarn garnet and pyroxene compositions (data from Wang, 2011; base map from Meinert, 1992).

CAGS, via in situ sampling of zircon volumes as small as 12, 25, and 40 μm in diameter and about 10 μm in depth. Before analysis, each sample surface was cleaned with ethanol to eliminate possible contamination. Every 10 sample analyses were followed by measurements of 1 sample of zircon 91,500, GJ 1, or NIST 612 standard. $^{207}Pb/^{206}Pb$ and $^{206}Pb/^{238}U$ were calculated using the ICPMSDataCal program (Andersen, 2002). The $^{207}Pb/^{235}U$ ratio was calculated from the values of $^{207}Pb/^{206}Pb$ and $^{206}Pb/^{238}U$ ($^{235}U = {}^{238}U/137.88$). The weighted mean U–Pb ages and concordia plots were processed using ISOPLOT program (Ludwig, 2001).

5.2. Molybdenite

5.2.1. Sample selection

Thirty-six molybdenite samples were collected from different ore types, comprising 5 from the hornfels, 12 from the skarn, and 19 from the porphyry. The molybdenite samples in the hornfels and porphyry were collected from a quartz–molybdenite vein in drill core. Ten of the skarn samples from the Lead Mountain open pit contain mainly disseminated molybdenite, and the other two samples were taken from a quartz–molybdenite vein in drill core (Table 5).

5.2.2. Methodology

Test-standard mono-mineral powders were selected in an indoor, pollution-free environment. Inductively coupled plasma–mass spectrometry (ICP–MS) was used to conduct isotope assay tests in the Re–Os isotope laboratory of the National Research Center for Geoanalysis, CAGS. For details of the chemical processing and mass spectrometric determination techniques, see Du et al. (2001, 2004).

6. Results

6.1. Zircon U–Pb dating

Most of the zircons (100–150 μm across) from the four samples are euhedral to subhedral, with elongate prismatic crystal shapes. The zircon grains show a strong symmetrical zoning in CL images. These characteristics suggest that the zircons from the igneous rocks are of magmatic origin. Fifteen spot analyses of zircons from sample TSCC-14 (QDP) yield concordant $^{206}Pb/^{238}U$ ages with a weighted mean age of 15.96 ± 0.5 Ma (MSWD = 2.2). Fourteen spot analyses of ZK813-1 (GDP) yield concordant $^{206}Pb/^{238}U$ ages with a weighted mean age of 15.72 ± 0.14 Ma (MSWD = 2.1). Eighteen spot analyses of ZK813-2 (MGP) yield concordant $^{206}Pb/^{238}U$ ages with a weighted mean age of

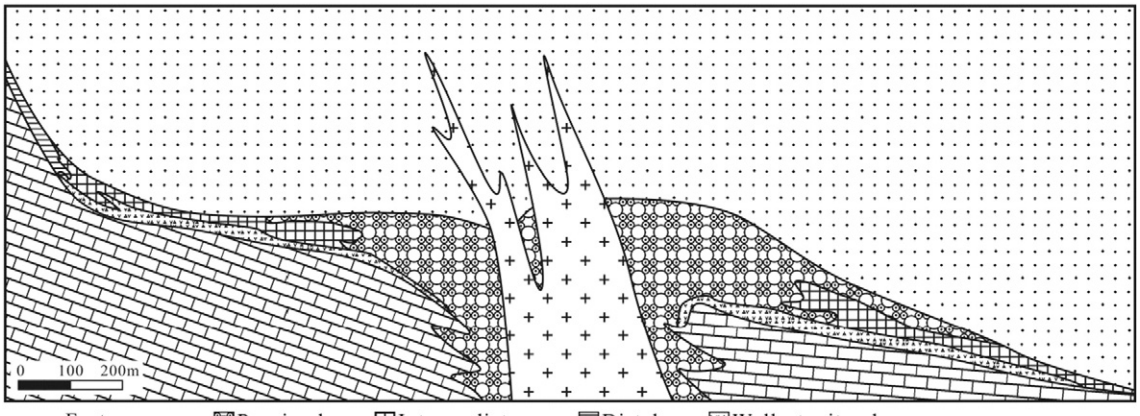

Feature	Proximal	Intermediate	Distal	Wollastonite skarn
Garnet:Pyroxene	>20:1	≈10:1	≈5:1	Wollastonite, lesser garnet and pyroxene
Garnet color	red-brown	brown-green	green-yellow	
Max Ad in garnet	>70%	40-70%	<40%	
Ore sulfides	Mol>Cpy+Bn	Bn+Cpy>Mol	Gn+Sph>Cpy+Bn	Bn>Cpy
(Pb+Zn)/%	<0.1%	<0.3%	1.5~3.0%	<0.3%
Cu/%	0.5~1.0%	1.0~1.5%	0.3~0.7%	1.5~3.0%
Mo/%	0.1~0.15%	0.03~0.07%	<0.03%	<0.01%

Geologic legend
Linbuzong Fm
Duodigou Fm
Porphyry

Fig. 10. Idealized zonation pattern for the 1# skarn orebody illustrating variations in mineralogy, composition, and metal ratios. Mol = molybdenite, Cpy = chalcopyrite, Bn = bornite, Sph = sphalerite, and Gn = galena.

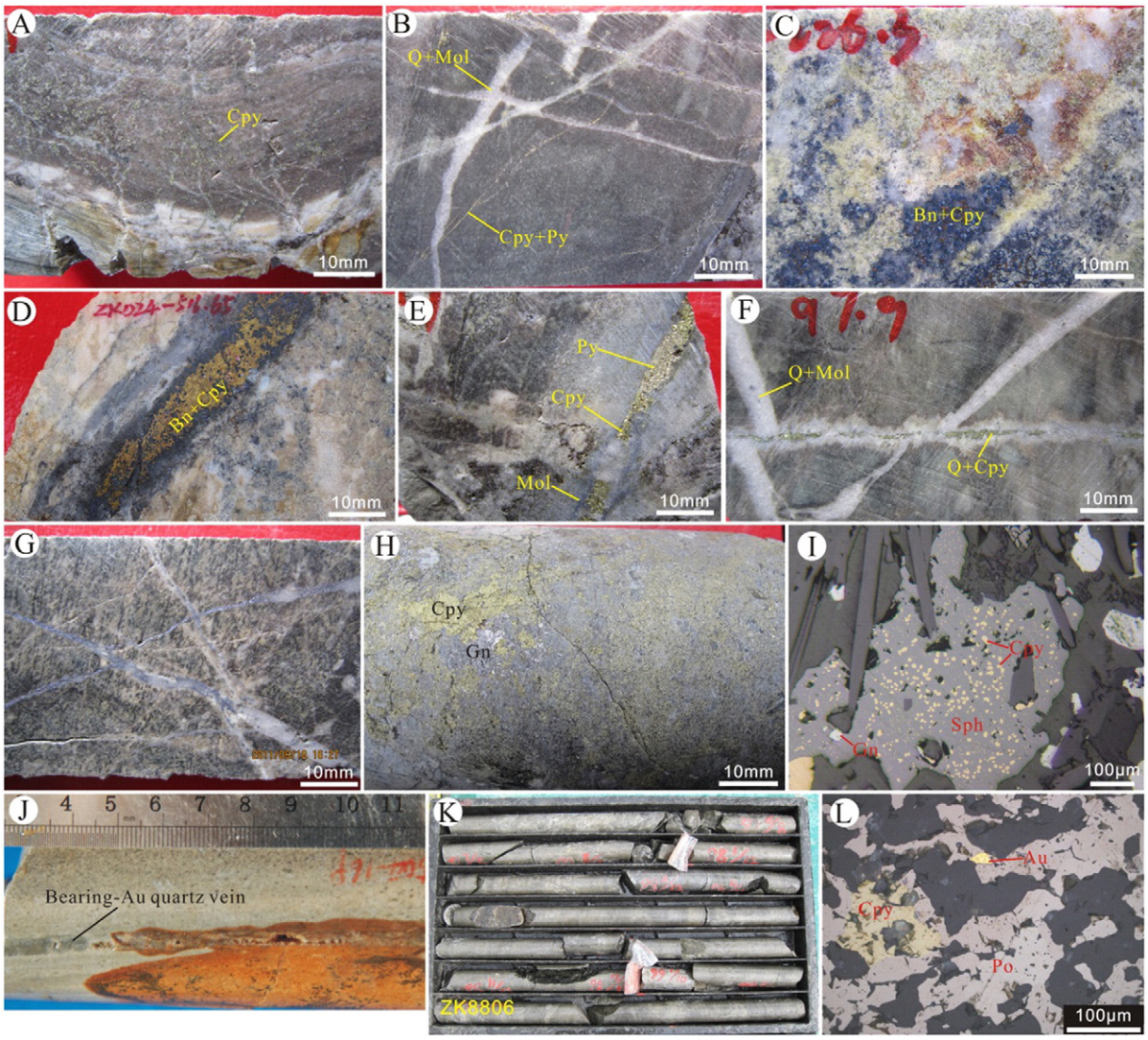

Fig. 11. Mineralization features of the Jiama Cu–polymetallic system. (A) Disseminated Cpy in the hornfels. (B) Stockwork Q-Mol cutting an early veinlet of Cpy + Py. (C) Disseminated Bn + Cpy in the skarn. (D) Vein Bn + Cpy in the skarn. (E) Vein Q + Mol + Py + Cpy in the hornfels. (F) Late-stage Q + Cpy veins cutting early Q + Mol veins in the hornfels. (G) Stockwork Q + Mol in the hornfels. (H) Massive Gn + Cpy + Sph in the skarn. (I) Cpy exsolution from Sph. (J) Au-bearing Q vein in the QDP. (K) Massive Po orebody (>20 m thick) in the ZK8806 drill core. (L) Densely disseminated Po with Cpy and native gold. Q = quartz, Cpy = chalcopyrite, Po = pyrrhotite, Py = pyrite, Mol = molybdenite, Gn = galena, Sph = sphalerite, and Bn = bornite.

15.59 ± 0.09 Ma (MSWD = 1.0). Eighteen spot analyses of ZK2414 (GP) yield concordant $^{206}Pb/^{238}U$ ages with a weighted mean age of 15.48 ± 0.08 Ma (MSWD = 0.64; Fig. 13).

6.2. Molybdenite Re–Os dating

The Re–Os isotopic results of the 36 molybdenite samples analyzed are listed in Table 5. The ^{187}Re content of molybdenite in the hornfels was 121.5–387.4 ppm, with an average of 276 ppm; the ^{187}Re content in the skarn was 123.7–1402.7 ppm, with an average of 796.8 ppm; and the ^{187}Re content of molybdenite in the porphyry was relatively low, at 42.9–130.5 ppm, with an average of 72.9 ppm. The variation in ^{187}Os content was similar to that of ^{187}Re content; i.e., relatively high in the hornfels and skarn, and relatively low in the porphyry. The model ages of molybdenite are in the range 14.2–15.5 Ma and all the ages are within error of each other. The isochron ages of the molybdenite in the hornfels, porphyry, and skarn, as calculated by the application software, are 14.67 ± 0.37 Ma (MSWD = 0.30), 14.66 ± 0.27 Ma (MSWD = 1.2), and 15.37 ± 0.15 Ma (MSWD = 0.19), respectively (Fig. 14).

7. Discussion

7.1. Geological significance of mineralization ages

The zircon U–Pb ages of the four ore-bearing porphyries from the ore district indicate that the general order of emplacement was QDP → GDP → MGP → GP (Fig. 13), within the period 16–15.5 Ma. The Re–Os dating shows that the age of molybdenite from the skarn is 15.37 Ma, whereas the molybdenite in the porphyry and the hornfels have ages of ~14.7 Ma, about 0.7 Ma later than the skarn. The close

Table 4
Distal Au mineralisation of the Jiama porphyry Cu-polymetallic system.

Wall-rock	Drill hole	Thickness/m	Au g/t	Ag g/t	Cu %	Mo %	Pb %	Zn %
Skarn	ZK4702	2.77	4.15	3.36	0.02	0	0	0
	ZK4703	7.76	6.68	12.22	0.11	0	0.01	0.01
	ZK8801	3.54	4.77	1.03	0.01	0	0	0
	ZK8806	15	4.98	3.87	0.5	0	0.01	0.17
QDP	ZK4504	10	17.15	5.06	0.01	0.01	0.01	0
		13.06	2.04	1.07	0.01	0	0	0.01

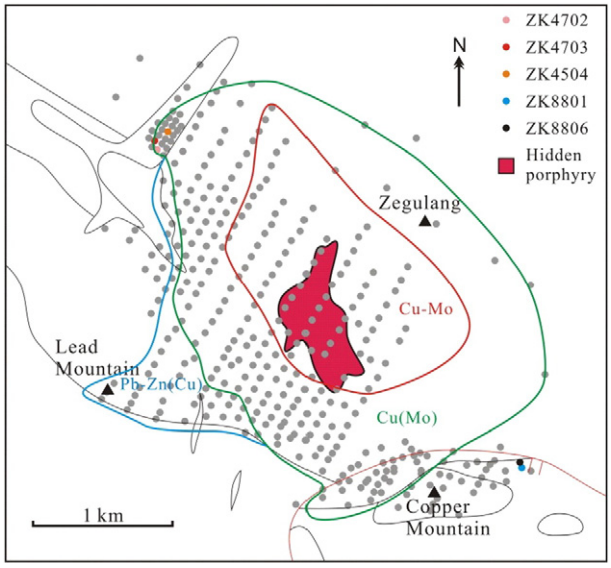

Fig. 12. Metal zoning in the skarn. The mineralization zoning outwards from the porphyry contact is Cu–Mo ± Au ± Ag → Cu ± Mo ± Au ± Ag → Pb–Zn ± Cu ± Au ± Ag → Au ± Ag.

relationship between the molybdenite and chalcopyrite indicates that the molybdenite Re–Os dates represent the timing of ore formation. Therefore, the ore-formation ages belong to the Langhian (Miocene).

The mineralization ages of the Jiama deposit are consistent with those of the large-scale deposits of Qulong, Bangpu, Tinggong, etc. (Table 2), which constitute a porphyry metallogenic belt distributed from east to west within the Gangdese Belt (Fig. 2b). The proven copper resources in this porphyry metallogenic belt exceed 30 million tons. The emplacement of porphyry in the belt was related to the extensional setting of the Gangdese Belt during the Miocene (Hou et al., 2004, 2015; Richards, 2015).

7.2. Sources of metals and sulfur

7.2.1. Source of metals

Much research has been conducted on the source of the metals in the ore district. The ratios of $^{206}Pb/^{204}Pb$, $^{207}Pb/^{204}Pb$, and $^{208}Pb/^{204}Pb$ in the sulfide minerals are 18.150–18.752, 15.480–15.686, and 38.850–39.135, respectively; in the ore-bearing porphyry are 17.344–18.765, 15.362–15.730, and 37.522–38.997, respectively; and in the limestone of the ore district are 17.28–17.38, 15.21–15.25, and 37.84–37.91, respectively (Guo et al., 2014). The lead isotopic composition of the sulfide minerals is similar to that in the ore-bearing porphyry, but is distinct from that in the limestone of the ore district. These results indicate that the ore-forming metals in the Jiama deposit were derived mainly from the ore-bearing porphyry, and therefore have the same source as the porphyry.

7.2.2. Source of sulfur

The $\delta^{34}S$ values of bornite, chalcopyrite, galena, sphalerite, and sulfates in the primary ore minerals range between 13.6‰ and 12.5‰,

Table 5
Re–Os data for molybdenite of the Jiama porphyry Cu-polymetallic system.

Rock type	Sample	Re[a] (ppm)	^{187}Re (ppm)	^{187}Os (ppb)	Age[b] (Ma)
Hornfels	JM1618-158.95	279.39 (2)	175.6 (1)	42.284 (0.3)	14.45 ± 0.2
	JM1618-163.76	566.41 (5)	356 (3)	87.206 (0.8)	14.70 ± 0.2
	JM1618-168.2	193.31 (2)	121.5 (1)	29.554 (0.3)	14.60 ± 0.2
	JM1618-179.1	540.03 (5)	339.4 (3)	82.608 (0.9)	14.61 ± 0.2
	JM1618-182	616.35 (6)	387.4 (4)	94.251 (0.8)	14.60 ± 0.2
Porphyry	JM2010-651b	126.19 (1)	79.3 (0.7)	19.392 (0.2)	14.67 ± 0.2
	JM2010-651c	101.66 (1)	63.9 (0.5)	15.121 (0.1)	14.20 ± 0.2
	JM2010-651d	207.67 (2)	130.5 (1)	32.637 (0.3)	15.01 ± 0.2
	JM2010-651.1a	130.63 (1)	82.1 (0.7)	19.981 (0.2)	14.61 ± 0.2
	JM2010-651.1b	137.06 (1)	86.1 (0.8)	21.035 (0.2)	14.65 ± 0.2
	JM2010-651.1c	123.18 (1)	77.4 (0.6)	18.996 (0.2)	14.73 ± 0.2
	JM2010-651.1d	144.12 (1)	90.6 (0.8)	22.284 (0.2)	14.76 ± 0.2
	JM2010-651.2a	137.32 (1)	86.3 (0.7)	20.559 (0.2)	14.30 ± 0.2
	JM2010-651.2c	122.12 (1)	76.8 (0.6)	18.593 (0.2)	14.54 ± 0.2
	JM2010-651.4a	118.76 (1)	74.6 (0.6)	18.317 (0.1)	14.73 ± 0.2
	JM2010-651.4b	129.17 (1)	81.2 (0.7)	19.931 (0.2)	14.73 ± 0.2
	JM2010-653.1a	101.99 (1)	64.1 (0.6)	15.787 (0.1)	14.78 ± 0.2
	JM2010-653.1b	93.1 (1)	58.5 (0.5)	14.551 (0.1)	14.92 ± 0.2
	JM2010-653.1c	86.6 (1)	54.4 (0.5)	13.311 (0.1)	14.68 ± 0.2
	JM2010-662.5a	68.26 (1)	42.9 (0.3)	10.447 (0.1)	14.62 ± 0.2
	JM2010-662.5b	90.05 (1)	56.6 (0.5)	14.06 (0.1)	14.91 ± 0.2
	JM2010-663a	73.55 (1)	46.2 (0.8)	11.552 (0.1)	15.00 ± 0.3
	JM2010-663b	126.96 (2)	79.8 (1)	19.764 (0.2)	14.86 ± 0.2
	JM2010-663c	84.41 (1)	53.1 (0.9)	13.087 (0.2)	14.80 ± 0.3
Skarn	YXK-01-1	1649.08 (15)	1036.5 (9)	264.2 (2.2)	15.30 ± 0.22
	YXK-01-2	1797.98 (21)	1130.1 (13)	286.7 (2.6)	15.23 ± 0.26
	YXK-01-3	1981.07 (19)	1245.1 (12)	317.0 (2.6)	15.28 ± 0.23
	YXK-01-4	2231.78 (19)	1402.7 (12)	362.3 (3.1)	15.50 ± 0.22
	YXK-01-5	1541.37 (13)	968.8 (8)	247.2 (2)	15.31 ± 0.22
	YXK-02-1	1625.85 (14)	1021.9 (9)	259.3 (2.2)	15.23 ± 0.22
	YXK-02-2	1303.94 (11)	819.6 (7)	209.5 (1.8)	15.34 ± 0.22
	YXK-04	382.54 (3)	240.4 (2)	61 (0.5)	15.23 ± 0.22
	YXK-06	1060.12 (8)	666.3 (5)	168.8 (1.5)	15.21 ± 0.22
	YXK-07	1168.39 (9)	734.4 (6)	186.6 (1.7)	15.25 ± 0.22
	JM2010-605.6	273.85 (2)	172.1 (1)	43.02 (0.4)	15.00 ± 0.2
	JM2010-607	196.88 (2)	123.7 (1)	30.647 (0.3)	14.86 ± 0.2

[a] Absolute uncertainties (in parentheses) are shown at the 2σ level for the last digit indicated.
[b] Ages were calculated using $^{187}Os = {}^{187}Re\ (e^{\lambda t} - 1)$ and include all analytical and ^{187}Re decay constant uncertainties; decay constant used for ^{187}Re is $1.666 \times 10^{-11}\ yr^{-1}$ (Smoliar et al., 1996).

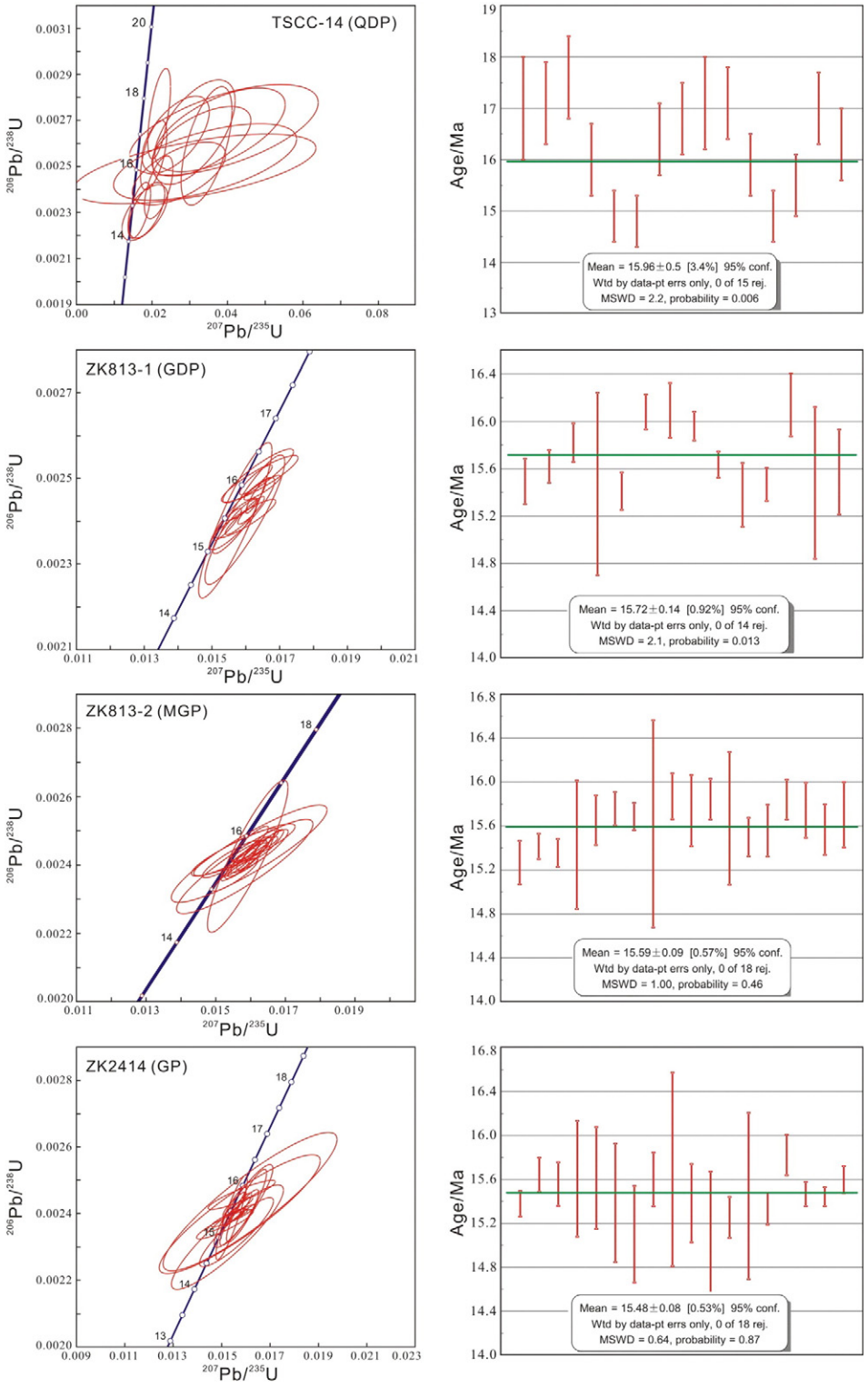

Fig. 13. Results of U–Pb LA-ICP-MS dating of detrital zircon from the porphyries.

with an average of 0.788‰ (Guo et al., 2014). The sulfur isotope composition conforms to a standardized normal distribution, mainly concentrated between −4‰ and 3.0‰ (Guo et al., 2014), indicating that the sulfur isotopes have undergone homogenization. The wide range of $\delta^{34}S$ values suggests that some metallic minerals may have incorporated sulfur from the crust. The distribution of sulfur isotopes is centered on zero, which is characteristic of mantle-derived sulfur.

7.3. Genesis of the Jiama porphyry

The $\varepsilon_{Nd}(t)$ values of the Jiama porphyry range between −3.9 and 0.8, and $(^{87}Sr/^{86}Sr)_i$ ranges between 0.70531 and 0.70762 (Tang et al., 2010). These values are similar to Sr–Nd isotopic compositions in the Cordillera Blanca (Petford and Atherton, 1996), and are consistent with a magma source in the upper mantle (Fig. 15A) and conditions of

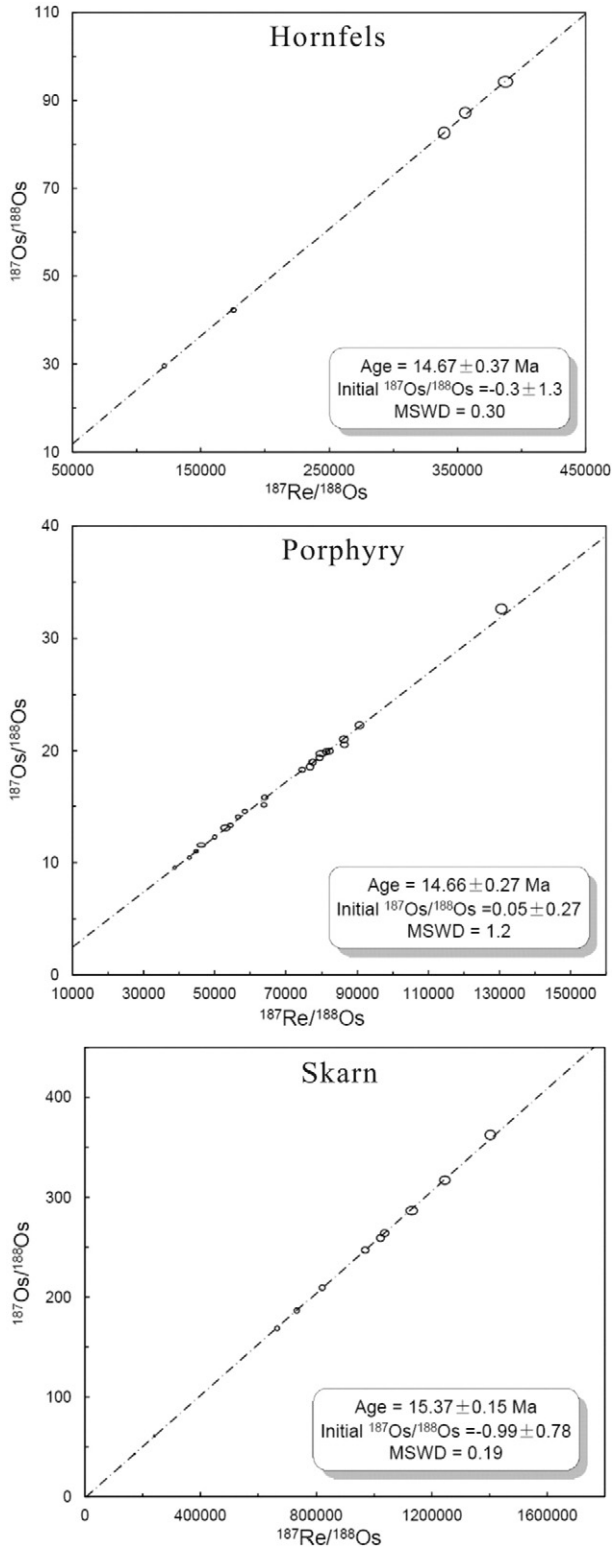

Fig. 14. Results of Re–Os dating of molybdenite from the hornfels, porphyry, and skarn.

medium to high oxygen fugacity (Fig. 15B). A post-collisional tectonic setting would promote a pressure decrease and rise of the asthenosphere to promote partial melting of the upper mantle and magma generation (Richards, 2009; Menzies and Chazot, 1995).

The porphyry has high Sr contents and moderate Eu anomalies (Fig. 4C, D), reflecting a magma source with no plagioclase, or a residual phase with no plagioclase. HFSE are strongly depleted, indicating that the magma source was water-bearing and contained residual garnet amphibolite eclogite and garnet amphibolite (Defant and Drummond, 1990; Drummond et al., 1996). The relative depletion in Yb and intense fractionation of the LREE with respect to the HREE are characteristic of this type of porphyry (Fig. 4C, D), and require 10%–25% partial melting of amphibole eclogite and garnet amphibolite (Defant and Drummond, 1990). The porphyry has a high initial Sr value, indicating an enriched mantle type II (EM II) component in the source (Fig. 15A). The characteristics of the peraluminous GP, which are similar to those of S-type granites (Table 3; Fig. 4B), suggest that the magma incorporated wall rock fragments during stoping. These fragments may have included sandy or argillaceous rocks, which would have affected the composition of the magma. Therefore, magmatic evolution at Jiama occurred not only via crystallization differentiation, but also through magma mixing and crustal contamination.

The above results on the genesis of the Jiama porphyry are similar to those of other porphyries formed between 20 and 12 Ma in the Gangdese Metallogenic Belt (Hou et al., 2004). The trace element features of the Jiama magmatic rocks are similar to those of the Yeba Formation island arc volcanic rocks (Fig. 4C, D), which raises the possibility that the Jiama magmatic rocks originated directly from partial melting of the Yeba Formation rocks.

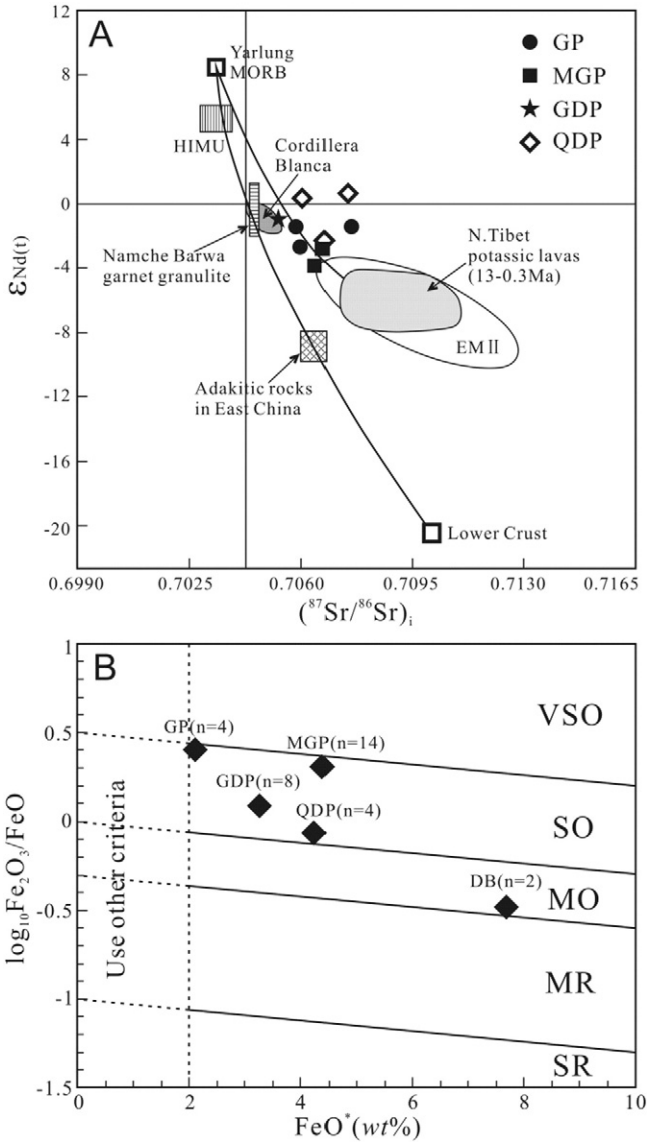

Fig. 15. (A) $\varepsilon_{Nd}(t)$ vs. $(^{87}Sr/^{86}Sr)_i$ diagram (modified from Hou et al., 2004) and (B) $\log_{10}Fe_2O_3/FeO$ vs. FeO^* (wt.%) diagram (Blevin, 2004) for the Jiama igneous rocks.

7.4. Genetic model

As the Indian–Asian continent shifted from the subduction stage to the continental collision stage during the Early Eocene, a thrust nappe structure was formed from north to south in the Jiama area. This formed a series of overturned folds with axial planes dipping to the north (Fig. 3). At the same time, a detachment fault caused sliding between the Linbuzong Formation sandstone and slate, and the Duodigou Formation limestone (owing to their contrast rock physical properties), which resulted in the formation of a large-scale interlayer detachment zone. The Copper Mountain gliding nappe was formed as the rock that was pushed to a higher position slipped northward as a result of gravitational instability (Zhong et al., 2012; Fig. 3).

During the Miocene, rifting in the Neo-Tethyan basin (Hou et al., 2004, 2015; Hou and Cook, 2009; Wang et al., 2014a; 2014b) placed the southern Gangdese in an extensional setting. The asthenosphere welled up or ascended diapirically, resulting in adiabatic decompression and partial melting of the upper mantle (Menzies and Chazot, 1995.) In the Langhian (Miocene), rising magma intruded along the Niumatang Anticline in the Jiama area (Fig. 3). Repeated intermediate–acidic porphyry emplacement occurred under the influence of crystallization, magma mixing, wall-rock contamination, magma chamber decompression, and fluid boiling (Burnham, 1979). Consequently, the following events occurred. (1) The emplacement of the porphyry released large amounts of heat, resulting in thermal metamorphism producing hornfels and marble from sandstone–slate and limestone, respectively (Fig. 1). (2) The mechanical force generated by porphyry emplacement and hydromagmatic explosions caused the hornfels to be crushed, forming a cylindrical fracture system (Burnham, 1979; Richards and Mumin, 2013). (3) The magma chamber exsolved magmatic–hydrothermal fluids and volatiles. (4) Under lithostatic to hydrostatic conditions, and driven by thermopower and regional tectonic stress, some of the magmatic–hydrothermal fluids and volatiles migrated vertically along the cylindrical fracture system to form the typical porphyry Cu zoned alteration pattern, as well as porphyry Cu–Mo mineralization (Fig. 16; Burnham, 1979; Fournier, 1987). The partial fluid diffused laterally along the interlayer detachment zone, aided by the upper strata that acted as a trap rock. Magmatic–hydrothermal fluids caused complete metasomatism of the marble in the lower Duodigou section and formed prograde skarn. Skarn formed as a result of interactions between hydrothermal fluid and wall rock (Fig. 16). (5) Subsequently, the incursion of meteoric water induced further metasomatism of the prograde skarn to form retrograde skarn and Cu, Mo, Pb, and Zn (±Au and Ag) mineralization, the zonation of which was influenced by the composition and temperature of the prograde skarn (Meinert, 1997; Meinert et al., 2005; Henley et al., 2015). In addition, the hydrothermal fluids deposited low-sulfidation epithermal Au within the extensional faults in the distal marble and slate (Zhong et al., 2011; Zheng et al., 2012b; Table 4; Fig. 16).

7.5. Implications for exploration

Exploration breakthroughs at the Jiama deposit have contributed to advances at other similar projects, such as Xingaguo, Mengyaa, and

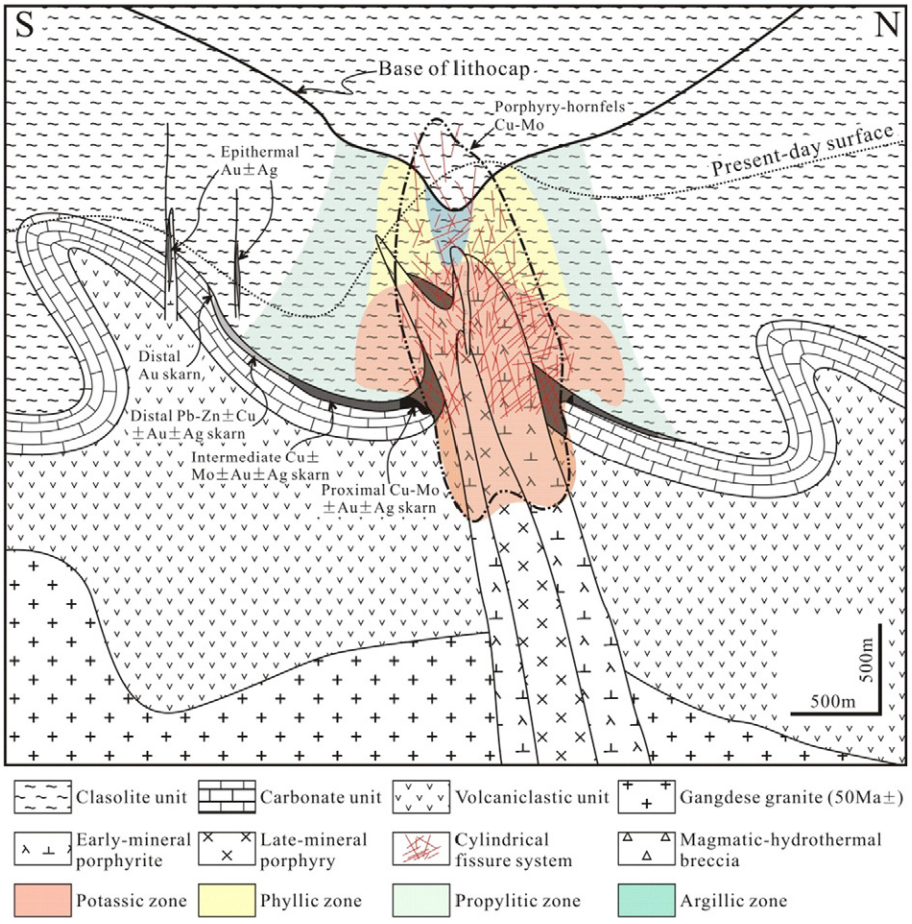

Fig. 16. Schematic model of the Jiama porphyry Cu–polymetallic system showing spatial interrelationships within a centrally located porphyry–hornfels Cu–Mo orebody in a multiphase porphyry stock, and its immediate host rocks. The peripheral proximal, intermediate, and distal skarn orebody and epithermal fault-zone-hosted Au orebody are indicated.

Yaguila. The layered skarn orebody that occurs at the Si–Ca interface (i.e., the detachment fault between clastic rocks and carbonate rocks) has become an important exploration target in the area, and significant efforts have been made at these mines to find this orebody (Fig. 17). For the purposes of exploration, the following are the most important ore-controlling geological conditions for prospecting in the area, according to the Jiama model.

(1) The combination of clastic-carbonate rocks. These two rocks may be of different ages or similar ages; e.g., the combination of the Linbuzong Formation and the Duodigou Formation, or the interbedded clastic-carbonate rocks in the Takela Formation and the Luobadui Formation (Fig. 17).
(2) A detachment zone that occurs between clastic rocks and carbonate rocks. Under the influence of India–Eurasia collision, a

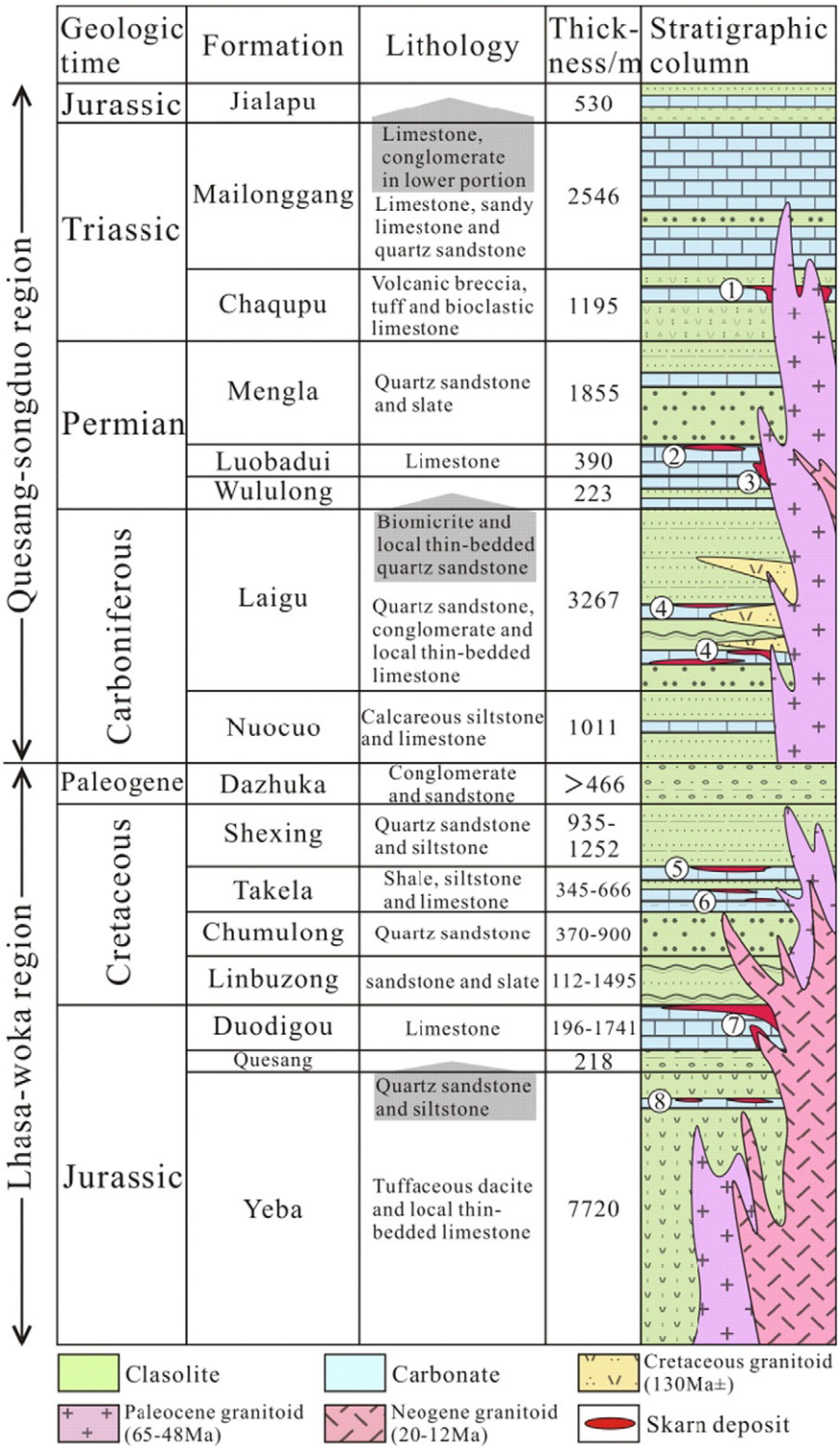

Fig. 17. Occurrence of skarn deposits in the Lhasa area: ① Lietinggang skarn deposit; ② Mengyaa skarn deposit; ③ Lawu skarn deposit; ④ Yaguila and Zedexiong skarn deposits; ⑤ Xingaguo skarn deposit; ⑥ Lunlang skarn deposit; ⑦ Jiama skarn deposit; ⑧ Zhibula skarn deposit.

widespread interlayer detachment developed along the contact between different lithologies in the eastern section of the Gangdese Metallogenic Belt, and this was affected by the thrust nappe structure.

(3) Extensive hornfels alteration of the clastic rocks. This resulted from the emplacement of magmatic rock of Paleocene–Eocene or Miocene in age (Fig. 17). The extent of the interlayered skarn is generally constrained by the extent of hornfels alteration.

If the three geological conditions mentioned above occur in a given area, it is likely that porphyry–skarn-type deposits, like the Jiama, would have developed. Prospecting should target porphyry Cu–Mo and skarn mineralization in the interlayer detachment zone.

8. Conclusions

(1) The Jiama deposit is the most characteristic, well-preserved porphyry Cu–polymetallic system identified in Tibet. It is composed of skarn Cu–polymetallic, hornfels Cu–Mo, and porphyry Mo ± Cu orebodies, and distal Au mineralization. The skarn Cu–polymetallic orebodies are controlled by the porphyry–carbonate contact zone and the hornfels–marble interlayer detachment zone, in which hornfels and porphyry Cu–Mo orebodies are mainly constrained by the fracture system caused by the emplacement of magmatic rock. Individual gold orebodies formed in extensional faults in the distal zone, and are the product of late-stage hydrothermal alteration.

(2) The Jiama deposit alteration includes the potassic, phyllic, propylitic and argillic zones typical of a porphyry Cu system, along with a lithocap and skarn alteration. Cu and Mo mineralization occurs mainly in the potassic and phyllic zones. The skarn shows a typical skarn alteration zonation from the porphyry contact zone outwards, reflected in the mineralogy and mineral chemical composition of garnet and pyroxene. The skarn hosts polymetallic mineralization.

(3) The emplacement age of the ore-bearing porphyries and the timing of metallogenesis of the deposit are both Langhian, in the Miocene (16–14 Ma). The emplacement of porphyry was controlled by the Niumatang Anticline, and the major ore-bearing porphyries were formed at medium to high oxygen fugacities. These porphyries are characterized by high-K calc-alkaline, quasi-aluminous, I-type granite compositions, HFSE depletion, LILE enrichment, and weak to moderate negative Eu anomalies indicate evolution by crystallization differentiation, magma mixing, and wall-rock contamination.

(4) The major finding of this study, that the layered skarn Cu–polymetallic orebody was controlled by the interlayer detachment zone formed by the north–south thrust nappe structure, has great significance for exploration in the numerous skarn-type deposits in the Lhasa area.

Conflict of interest

No conflict of interest.

Acknowledgments

This research was supported by the National Science Foundation of China (41302060), the Program of the China Geological Survey (12120114050501, 12120113093700). We are grateful to all members of the Jiama project team for their work. We thank Prof. Franco Pirajno and Dr. Greg Corbett for help with the manuscript. Finally, we thank an anonymous reviewer and the editors for insightful comments that improved this paper.

References

Andersen, T., 2002. Correction of common lead in U–Pb analyses that do not report ^{204}Pb. Chem. Geol. 192, 59–79.
Blevin, P.L., 2004. Redox and compositional parameters for interpreting the granitoid metallogeny of Eastern Australia: implications for gold–rich ore systems. Resour. Geol. 54, 241–252.
Burnham, C.W., 1979. Magmas and hydrothermal fluids. In: Barnes, H.L. (Ed.), Geochemistry of Hydrothermal ore Deposits, 2nd ed. John Wiley and Sons, New York, pp. 71–136.
Collins, W.J., Beams, S.D., White, A.J.R., Chappell, B.W., 1982. Nature and origin of A-type granites with particular reference to southeastern Australia. Contrib. Mineral. Petrol. 80, 189–200.
Chung, S.L., Chu, M.F., Zhang, Y.Q., Xie, Y.W., Lo, C.H., Lee, T.Y., Lan, C.Y., Li, X.H., Zhang, Q., Wang, Y.Z., 2005. Tibetan tectonic evolution inferred from spatial and temporal variations in post–collisional magmatism. Earth-Sci. Rev. 68, 173–196.
Chung, S.L., Chu, M.F., Ji, J.Q., O'Reilly, S.Y., Pearson, N.J., Liu, D.Y., Lee, T.Y., Lo, C.H., 2009. The nature and timing of crustal thickening in southern Tibet: geochemical and zircon Hf isotopic constraints from postcollisional adakites. Tectonophysics 477, 36–48.
Defant, M.J., Drummond, M.S., 1990. Derivation of some modern arc magmas by melting of young subducted lithosphere. Nature 347, 662–665.
Drummond, M.S., Defant, M.J., Kepezhinskas, P.K., 1996. Petrogenesis of slab–derived trondhjemite–tonalite–dacite/adakite magmas. Trans. R. Soc. Edinb. Earth Sci. 87, 205–215.
Du, A.D., Zhao, D.M., Wang, S.X., Sun, D.Z., Liu, D.Y., 2001. Precise Re–Os dating for molybdenite by ID–NTIMS with Carius tube sample preparation. Rock and Mineral Analysis 20, 247–252 (in Chinese with English abs.).
Du, A.D., Wu, S.Q., Sun, D.Z., Wang, S.X., Qu, W.J., Markey, R., Stein, H., Morgan, J., Malinovskiy, D., 2004. Preparation and certification of Re–Os dating reference materials: molybdenites HLP and JDC. Geostand. Geoanal. Res. 28, 41–52.
Du, D.D., Qu, X.M., Wang, G.H., Xin, H.B., Liu, Z.B., 2011. Bidirectional subduction of the Middle Tethys oceanic basin in the west segment of Banggonghu–Nujiang suture, Tibet: evidence from zircon U–Pb LAICPMS dating and petrogeochemistry of arc granites. Acta Petrologica Sinica 27, 1993–2002 (in Chinese with English abs.).
Duan, J.L., Tang, J.X., Mason, R., Zheng, W.B., Ying, L.J., 2014. Zircon U–Pb age and deformation characteristics of the Jiama porphyry copper deposit, Tibet: implications for relationships between mineralization, structure and alteration. Resour. Geol. 64, 316–331.
Fournier, R.O., 1987. Conceptual models of brine evolution in magmatic–hydrothermal systems. U.S. Geol. Surv. Prof. Pap. 1350, 1487–1506.
Gao, Y.M., Chen, Y.C., Tang, J.X., Li, C., Li, X.F., Gao, M., Cai, Z.C., 2011. Re–Os dating of molybdenite from the Yaguila porphyry molybdenum deposit in Gongbujiangda area, Tibet, and its geological significance. Geological Bulletin of China 30, 1027–1036 (in Chinese with English abs.).
Gao, Y.M., Chen, Y.C., Tang, J.X., Luo, M.C., Leng, Q.F., Wang, L.Q., Yang, H.R., Pubu, C.R., 2012. A study of diagenetic and metallogenic geochronology of the Dabu Cu(Mo) deposit in Quxur county of Tibet and its geological implications. Acta Geoscientica Sinica 33, 613–623 (in Chinese with English abs.).
Guo, W.B., Zheng, W.B., Tang, J.X., Ying, L.J., Wang, Y.Y., Lin, B., 2014. Geochemical constraints on the source of metallogenic fluids and materials in the Jiama polymetallic Cu deposit, Tibet. Geology in China 41, 510–528 (in Chinese with English abs.).
Henley, R.W., King, P.L., Wykes, J.L., Renggli, C.J., Brink, F.J., Clark, D.A., Troitzsch, U., 2015. Porphyry copper deposit formation by sub–volcanic sulphur dioxide flux and chemisorption. Nat. Geosci. 8, 210–215.
Hou, Z.Q., Gao, Y.F., Qu, X.M., Rui, Z.Y., Mo, X.X., 2004. Origin of adakitic intrusives generated during mid–Miocene east–west extension in southern Tibet. Earth Planet. Sci. Lett. 220, 139–155.
Hou, Z.Q., Cook, N.J., 2009. Metallogenesis of the Tibetan collisional orogeny: a review and introduction to the special issue. Ore Geol. Rev. 36, 2–24.
Hou, Z.Q., Zheng, Y.C., Yang, Z.M., Rui, Z.Y., Zhao, Z.D., Jiang, S.H., Qu, X.M., Sun, Q.Z., 2013. Contribution of mantle components within juvenile lower–crust to collisional zone porphyry Cu systems in Tibet. Mineral. Deposita 48, 173–192.
Hou, Z.Q., Yang, Z.M., Lu, Y.J., Kemp, A., Zheng, Y.C., Li, Q.Y., Tang, J.X., Yang, Z.S., Duan, L.F., 2015. A genetic linkage between subduction– and collision–related porphyry Cu deposits in continental collision zones. Geology 43, 247–250.
Ji, X.H., Meng, X.J., Yang, Z.S., Zhang, Q., Tian, S.H., Li, Z.Q., Liu, Y.C., Yu, Y.S., 2014. The Ar–Ar geochronology of sericite from the cryptoexplosive breccia type Pb–Zn deposit in Narusongduo, Tibet and its geological significance. Geology and Exploration 50, 281–290 (in Chinese with English abs.).
Lang, X.H., 2012. Metallogenesis and metallogenic prediction for Xiongcun porphyry copper–gold district, Tibet. Unpublished Ph.D. Dissertation, Chengdu University of Technology, Chengdu, 189 pp (in Chinese with English abs.).
Lang, X.H., Tang, J.X., Li, Z.J., Huang, Y., Ding, F., Yang, H.H., Xie, F.W., Zhang, L., Wang, Q., Zhou, Y., 2014. U–Pb and Re–Os geochronological evidence for the Jurassic porphyry metallogenic event of the Xiongcun district in the Gangdese porphyry copper belt, southern Tibet, PRC. J. Asian Earth Sci. 79, 608–622.
Le Maitre, R.W., 2002. A Classification of Igneous Rock and Glossary of Terms. 2nd ed. Cambridge University, New York, pp. 1–236.
Leng, C.B., Zhang, X.C., Zhong, H., Hu, R.Z., Zhou, W.D., Li, C., 2013. Re–Os molybdenite ages and zircon Hf isotopes of the Gangjiang porphyry Cu–Mo deposit in the Tibetan Orogen. Mineral. Deposita 48, 585–602.
Leng, Q.F., Tang, J.X., Zheng, W.B., Zhang, J.S., Tang, P., Yan, G., Dong, Y., 2015. Re–Os dating of molybdenite from the Lakange porphyry Cu–Mo deposit in Tibet and its geological significance. Geology in China 42, 570–584, (in Chinese with English abs.).
Li, X.F., Wang, C.Z., Mao, W., Xu, Q.H., Liu, Y.H., 2014. The fault–controlled skarn W–Mo polymetallic mineralization during the main India–Eurasia collision: example from Hahaigang deposit of Gangdese metallogenic belt of Tibet. Ore Geol. Rev. 58, 27–40.

Ludwig, K.R., 2001. Eliminating mass–fractionation effects on U–Pb isochron ages without double spiking. Geochim. Cosmochim. Acta 65, 3139–3145.
Mao, J.W., Pirajno, F., Lehmann, B., Luo, M.C., Berzina, A., 2014. Distribution of porphyry deposits in the Eurasian continent and their corresponding tectonic settings. J. Asian Earth Sci. 79, 576–584.
Meinert, L.D., 1992. Skarns and skarn deposits. Geosci. Can. 19, 145–162.
Meinert, L.D., 1997. Application of skarn deposit zonation models to mineral exploration. Explor. Min. Geol. 6, 185–208.
Meinert, L.D., Dipple, G.M., Nicolescu, S., 2005. World skarn deposits. Economic Geology 100th Anniversary Volume, pp. 299–336.
Meng, X.J., Hou, Z.Q., Gao, Y.F., Huang, W., Qu, X.M., Qu, W.J., 2003. Re–Os dating for molybdenite from Qulong porphyry copper deposit in Gangdese metallogenic belt, Xizang and its metallogenic significance. Geological Review 49, 660–666 (in Chinese with English abs.).
Menzies, M.A., Chazot, G., 1995. Fluid processes in diamond to spinel facies shallow mantle. J. Geodyn. 20, 387–415.
Mo, X.X., Zhao, Z.D., Zhou, S., Dong, G.C., Guo, T.Y., Wang, L.L., 2002. Evidence for timing of the initiation of India–Asia collision from igneous rocks in Tibet. EOS Trans. 83, 47.
Mo, X.X., Hou, Z.Q., Niu, Y.L., Dong, G.C., Qu, X.M., Zhao, Z.D., Yang, Z.M., 2007. Mantle contributions to crustal thickening during continental collision: evidence from Cenozoic igneous rocks in southern Tibet. Lithos 96, 225–242.
Pan, G.T., Wang, L.Q., Li, S.R., Yuan, S.H., Ji, W.H., Yin, F.G., Zhang, W.P., Wang, B.D., 2012. Tectonic evolution of the Qinghai–Tibet Plateau. J. Asian Earth Sci. 53, 3–14.
Petford, N., Atherton, M., 1996. Na–rich partial melts from newly underplated basaltic crust: the Cordillera Blanca batholith, Peru. J. Petrol. 37, 1491–1521.
Richards, J.P., 2009. Postsubduction porphyry Cu–Au and epithermal Au deposits: products of remelting of subduction–modified lithosphere. Geology 37, 247–250.
Richards, J.P., Mumin, A.H., 2013. Magmatic–hydrothermal processes within an evolving earth: iron oxide–copper–gold and porphyry Cu ± Mo ± Au deposits. Geology 41, 767–770.
Richards, J.P., 2015. Tectonic, magmatic, and metallogenic evolution of the tethyan orogen: from subduction to collision. Ore Geol. Rev. 70, 323–345.
Rui, Z.Y., Li, G.M., Zhang, L.S., Wang, L.S., 2004. The response of porphyry copper deposits to important geological events in Xizang. Earth Science Frontiers 11, 145–152 (in Chinese with English abs.).
Sillitoe, R.H., 2010. Porphyry copper systems. Econ. Geol. 105, 3–41.
Smoliar, M.I., Walker, R.J., Morgan, J.W., 1996. Re-Os isotope constraints on the age of Group IIA, IIIA, IVA, and IVB iron meteorites. Science 271, 1099–1102.
Sun, S.S., McDonough, W.F., 1989. Chemical and isotope systematics of oceanic basalts: implications for mantle composition and processes. In: Saunders, A.D. (Ed.), Magmatism in Ocean Basins. Geological Society Publication 42, pp. 313–345.
Sun, X., Zheng, Y.Y., Wu, S., You, Z.M., Wu, X., Li, M., Zhou, T.C., Dong, J., 2013. Mineralization age and petrogenesis of associated intrusions in the Mingze–Chengba porphyry–skarn Mo–Cu deposit. Gangdese. Acta Petrologica Sinica 29, 1392–1406 (in Chinese with English abs.).
Tafti, R., Mortensen, J.K., Lang, J.R., Rebagliati, C.M., Oliver, J.L., 2009. Jurassic U–Pb and Re–Os ages for the newly discovered Xietongmen Cu–Au porphyry district, Tibet, PRC: implications for metalogenic epochs in the southern Gangdese belt. Econ. Geol. 104, 127–136.
Tafti, R., Lang, J.R., Mortensen, J.K., Oliver, J.L., Rebagliati, C.M., 2014. Geology and geochronology of the xietongmen (Xiongcun) Cu–Au porphyry district, Southern Tibet, China. Econ. Geol. 109, 1967–2001.
Tang, J.X., Chen, Y.C., Wang, D.H., Wang, C.H., Xu, Y.P., Qu, W.J., Huang, W., Huang, Y., 2009. Re–Os dating of molybdenite from the Sharang porphyry molybdenite deposit in Gongbujiangda County, Tibet and its geological significance. Acta Geologica Sinica 83, 698–704 (in Chinese with English abs.).
Tang, J.X., Wang, D.H., Wang, X.W., Zhong, K.H., Ying, L.J., Zheng, W.B., Li, F.J., Guo, N., Qin, Z.P., Yao, X.F., Li, L., Wang, Y., Tang, X.Q., 2010. Geological features and metallogenic model of the Jiama copper–polymetallic deposit in Tibet. Acta Geoscientica Sinica 31, 1–12 (in Chinese with English abs.).
Tang, J.X., Duo, J., Liu, H.F., Lang, X.H., Zhang, J.S., Zheng, W.B., Ying, L.J., 2012. Minerogenetic series of ore deposit in the east part of the Gangdise Metallogenic Belt. Acta Geoscientica Sinica 33, 393–410 (in Chinese with English abs.).
Tang, J.X., Zheng, W.B., Chen, Y.C., Wang, D.H., Ying, L.J., Qin, Z.P., 2013a. The deep porphyry prospecting breakthrough and its significance in the Jiama copper polymetallic deposit, Tibet. Journal of Jilin University (Earth Science Edition) 43, 1100–1110 (in Chinese with English abs.).
Tang, J.X., Zhang, Z., Li, Z.J., Sun, Y., Yao, X.F., Hu, Z.H., Wang, H.X., Song, J.L., He, L., 2013b. The metallogensis, deposit model and prospecting direction of the Ga'erqiong–Galale copper–gold ore Field, Tibet. Acta Geoscientica Sinica 34, 385–394 (in Chinese with English abs.).
Wang, B.D., Xu, J.F., Chen, J.L., Zhang, X.G., Wang, L.Q., Xia, B.B., 2010. Petrogenesis and geochronology of the ore–bearing porphyritic rocks in Tangbula porphyry molybdenum–copper deposit in the eastern segment of the Gangdese metallogenic belt. Acta Petrologica Sinica 26, 1820–1832 (in Chinese with English abs.).
Wang, B.D., Guo, L., Wang, L.Q., Li, B., Huang, H.X., Chen, F.Q., Duan, Z.M., Zeng, Q.G., 2012a. Geochronology and petrogenesis of the ore–bearing pluton in Chagele deposit in middle of the Gangdese metallogenic belt. Acta Petrologica Sinica 28, 1647–1662 (in Chinese with English abs.).
Wang, Z.H., Liu, Y.L., Liu, H.F., Guo, L.S., Zhang, J.S., Xu, K.F., 2012b. Geochronology and geochemistry of the Bangpu Mo–Cu porphyry ore deposit, Tibet. Ore Geol. Rev. 46, 95–105.
Wang, H., 2011. The study on mineralogical characteristics and its genetic implications of Jiama copper polymetallic deposit, Tibet. Unpublished Article on Master, Chinese Academy of Geological Sciences, Beijing, 100 pp (in Chinese with English abs.).
Wang, R., Richards, J.P., Hou, Z.Q., Yang, Z.M., DuFrane, S.A., 2014a. Increased magmatic water content–the key to oligo–Miocene porphyry Cu–Mo ± Au formation in the eastern Gangdese belt, Tibet. Econ. Geol. 109, 1315–1340.
Wang, R., Richards, J.P., Hou, Z.Q., Yang, Z.M., Gou, Z.B., DuFrane, A., 2014b. Increasing magmatic oxidation state from Paleocene to Miocene in the eastern gangdese belt, Tibet: implication for collision-related porphyry Cu–Mo ± Au mineralization. Econ. Geol. 109, 1943–1965.
Wang, Y.H., Wang, K.Q., Yu, W.Q., Huang, H., Wu, X.Q., 2006. Re–Os isotopic ages of tungsten–molybdenum (bismuth) poly–metallic ore deposit in the Jiagang Snowy Mountain, shenzha county, Tibet and the implications. Geology of Anhui 16, 112–117 (in Chinese with English abs.).
Wang, L.Q., Tang, J.X., Deng, J., Kang, H.R., Lin, X., Cheng, W.B., Li, Z., Zhang, Z., 2015. The Longmala and Mengya'a skarn Pb–Zn deposits, Gangdese region, Tibet: evidence from U–Pb and Re–Os geochronology for formation during early India–Asia collision. Int. Geol. Rev. 57, 1825–1842.
Xu, Z.Q., Yang, W.C., Ji, S.C., Zhang, Z.M., 2009. Deep root of a continent–continent collision belt: evidence from the Chinese Continental Scientific Drilling (CCSD) deep borehole in the Sulu ultrahigh–pressure (HPUHP) metamorphic terrane, China. Tectonophysics 475, 202–217.
Yan, X.Y., Huang, S.F., Du, A.D., 2010. Re–Os ages of large tungsten, copper and molybdenum deposit in the Zetang orefield, Gangdise and marginal strike–slip transforming metallogenesis. Acta Geologica Sinica 84, 398–406 (in Chinese with English abs.).
Yang, Y., Duo, J., Liu, H.F., Zhang, J.S., Wang, L.Q., Zhang, Z., Hu, Z.H., 2014. Re–Os dating of molybdenite from the Lietinggang iron polymetallic deposit of Tibet and its geological significance. Geology in China 41, 1554–1564 (in Chinese with English abs.).
Yang, Z.M., Hou, Z.Q., White, N.C., Chang, Z.S., Li, Z.Q., Song, Y.C., 2009. Geology of the post–collisional porphyry copper–molybdenum deposit at Qulong, Tibet. Ore Geol. Rev. 36, 133–159.
Yin, A., Harrison, T.M., Ryerson, F.J., Chen, W.J., Kidd, W.S.F., Copeland, P., 1994. Tertiary structural evolution of the Gangdese thrust system, southeastern Tibet. J. Geophys. Res. 99, 18175–18201.
Yin, A., Harrison, T.M., 2000. Geologic evolution of the Himalayan–Tibetan Orogen. Annu. Rev. Earth Planet. Sci. 28, 211–280.
Ying, L.j., Wang, C.H., Tang, J.X., Wang, D.H., Qu, W.J., Li, C., 2014. Re–Os systematics of sulfides (chalcopyrite, bornite, pyrite and pyrrhotite) from the Jiama Cu–Mo deposit of Tibet, China. J. Asian Earth Sci. 79, 497–506.
Zhao, Y.Y., Song, L., Fan, X.T., Shi, D.H., Zhang, T.P., Chen, H.Q., Qu, W.J., 2009. Re_2Os dating of molybdenite from the Shesuo copper polymetallic ore in Shenzha county, Tibet and its geological significance. Acta Geologica Sinica 83, 1150–1158 (in Chinese with English abs.).
Zhao, Z., Hu, D.G., Wu, Z.H., Lu, L., 2012. Molybdenite Re–Os isotopic dating of Sangbujiala copper deposit in the south margin of the Eastern Gangdese section and its geological implications. Journal of Geomechanics 18, 178–186 (in Chinese with English abs.).
Zheng, W.B., Tang, J.X., Chang, Z.S., Li, F.J., Yao, X.F., 2010. Geological and geochemical characteristics and genesis of the Jiama polymetallic copper deposit in Tibet. Geology and Exploration 46, 985–992 (in Chinese with English abs.).
Zheng, W.B., 2012a. The study on metallogenic model and prospecting pattern for the Jiama polymetallic copper deposit, Tibet. Unpublished Ph.D. Dissertation, Chengdu University of Technology, Chengdu, 219 pp (in Chinese with English abs.).
Zheng, W.B., Tang, J.X., Wang, X.W., Wang, H., Ying, L.J., Zhong, Y.F., Zhong, W.T., 2012b. Analysis on gold metallization in Jiama copper polymetallic deposit, Tibet. Journal of Jilin University (Earth Science Edition) 42, 181–197 (in Chinese with English abs.).
Zheng, Y.C., Hou, Z.Q., Gong, Y.L., Liang, W., Sun, Q.Z., Zhang, S., Fu, Q., Huang, K.X., Li, Q.Y., Li, W., 2014a. Petrogenesis of cretaceous adakite–like intrusions of the Gangdese plutonic belt, Southern Tibet: implications for mid–ocean ridge subduction and crustal growth. Lithos 190–191, 240–263.
Zheng, Y.Y., Sun, X., Gao, S.B., Zhao, Z.D., Zhang, G.Y., Wu, S., You, Z.M., Li, J.D., 2014b. Multiple mineralization events at the Jiru porphyry copper deposit, Southern Tibet: implications for Eocene and Miocene magma sources and resource potential. J. Asian Earth Sci. 79, 842–857.
Zheng, Y.Y., Zhang, G.Y., Xu, R.K., Gao, S.B., Pang, Y.C., Cao, L., Du, A.D., Shi, Y.R., 2007. Age limit of ore–forming and rock–forming in Zhunuo porphyry copper deposit, Gangdese, Tibet. Chin. Sci. Bull. 52, 2542–2548 (in Chinese).
Zhong, K.H., Li, L., Zhou, H.W., Bai, J.G., Li, W., Zhong, W.T., Zhang, Y.Q., Lan, J.Q., Zheng, F.S., Huang, X.Y., Lu, B., Lei, B., 2012. Features of Jiama–Kajunguo thrust–gliding nappe tectonic system in Tibet. Acta Geoscientica Sinica 33, 411–423 (in Chinese with English abs.).
Zhong, Y.F., Tang, J.X., Zhong, K.H., Ying, L.J., Deng, S.L., 2011. Preliminary study on the occurrence state of Au in Jiama copper–polymetallic deposit, Tibet. Journal of Chengdu University of Technology (Science and Technology Edition) 38, 298–305 (in Chinese with English abs.).
Zhu, D.C., Pan, G.T., Chung, S.L., Liao, Z.L., Wang, L.Q., Li, G.M., 2008. SHRIMP zircon age and geochemical constrains on the origin of Lower Jurassic volcanic rocks from the Yeba Formation, Southern Gangdese, South Tibet. International Geology Reviews 50, 442–471.
Zhu, D.C., Pan, G.T., Zhao, Z.D., Lee, H.Y., Kang, Z.Q., Liao, Z.L., Wang, L.Q., Li, G.M., Dong, G.C., Liu, B., 2009. Early cretaceous subduction–related adakite–like rocks in the Gangdese, south Tibet: products of slab melting and subsequent melt–peridotite interaction? J. Asian Earth Sci. 34, 298–309.
Zhu, D.C., Zhao, Z.D., Niu, Y.L., Mo, X.X., Chung, S.L., Hou, Z.Q., Wang, L.Q., Wu, F.Y., 2011. The Lhasa Terrane: record of a microcontinent and its histories of drift and growth. Earth Planet. Sci. Lett. 301, 241–255.